Electronic Supporting Information

Enhanced Easy Axis Magnetic Anisotropy in a Siloxane Bridged Linear Co^{II}_3 Single-Molecule Magnet

Madhuri Bhattacharya,[a] Sunil Kumar,[a] Björn Schwarz,[b*] Liviu Ungur,[c*] Kartik Chandra Mondal[a*]

[a] Department of Chemistry, Indian Institute of Technology Madras, Chennai 600036, India. E-mail: csdkartik@iitm.ac.in

[b] Institute for Applied Materials (IAM), Karlsruhe Institute of Technology (KIT), Hermann-von-Helmholtz-Platz 1, 76344 Eggenstein-Leopoldshafen, Germany. Email: bjoern.schwarz@kit.edu

[c] Office: MD1-05-03A, Department of Chemistry, National University of Singapore, Singapore. Email: chmlu@nus.edu.sg

Table of Contents

1. Magnetic and structural parameters comparison of the reported trinuclear Co^{II}_3 complexes

Table S1. Magnetic and structural parameters comparison of the reported trinuclear Co^{II} complexes. The dc magnetic experiments are recorded at H_{dc} = 1000 Oe field for all the reported complexes.[#]

No.	Complex	Geometry	Shortest intramolecular Co···Co distance (Å)	Shortest intermolecular Co···Co distance (Å)	Co(1)—L—Co(2) bridging angle (°)	J (cm^{-1})	$\chi_m T$ (cm^3 mol^{-1} K) at rt	D (cm^{-1})	U_{eff} (cm^{-1})[a]	τ_0 (s)	Reference
1	$[Co_3(N_3)_3(O_2CMe)_3(py)_5]$	Oh	3.146	7.051	90–125	-	11.25	-	-	-	1
2	$[\{Co(\mu\text{-}N_3O_3L)\}_2Co]$	Oh	2.909	5.818	88.32(8)	-6.38	8.45	-146.0	30.4(1)	6.6×10^{-8}	2
3	$\{[Co_3(pymp)_4(MeOH)_2][BPh_4]_2\}\cdot 2MeOH$	Oh	3.036	8.541	94.30(0)	+2.4	8.95	-6.5	18.0(2)	1.9×10^{-8}	3
4	$[Co_3(pymp)_4(pya)_2][ClO_4]_2$	Oh	3.049	7.351	92.19(10)	+0.65	8.70	-2.3	7.9(1)	8.5×10^{-8}	3
5	$[Co_3(N_3)_2(bca)_4(phen)_2]$	Oh (central), TBP (terminal)	3.120	-	94.0(2)	+4.15	7.94	-	-	-	4
6	$[Co_3(N_3)_2(bdc)_2(phen)_2]_n$	Oh (central), TBP (terminal)	3.230	10.616	103.07(8)	+7.85	7.64	-	-	-	4
7	$[Co_3(dpa)_2(Hdpa)_2(1\text{-}MeIm)_2(H_2O)_2]$	Oh (central), Sq. Py (terminal)	3.217	5.712	102.8 and 91.7	+1.4	-	-	-	-	5
8	$[\{CoN(SiMe_3)_2(\mu\text{-}\eta\text{-}[o\text{-}C_6H_4(k NSi^iPr_3)_2])\}_2Co]$	Sandwiched (central), TP (terminal)	4.585	-	-	+8.3	9.36	-	33.8(4)	4.4×10^{-9}	6
9	$[Co_3(\mu\text{-}OAc_F)_4(\mu\text{-}BA)_2(tmen)_2]$	Oh	3.550	-	118.5	-3.1	8.80	-	-	-	7
10	$[Co_3(phen)_3(L1)_2]$	Oh	3.656	10.213	119.2	-5.5	7.50	-	-	-	8
11	$[Co_3(\mu\text{-}OH)_2(\mu\text{-}pdz)_4(pdz)_2(NO_3)_2(H_2O)_2]\cdot(NO_3)_2\cdot(THF)\cdot 2(MeOH)$	Oh	3.240	7.040	114.8	-9.4	5.19	-	-	-	9
12	$Co_3(\mu\text{-}pdz)_4(\mu\text{-}NCS)_2(pdz)_2(NCS)_4]\cdot 2MeOH$	Oh	3.430	8.550	105.1	-6.1	8.07	-	-	-	9
13	$[Co_3(pytag)(py)_6Cl_3]ClO_4$	Oh	5.125	7.304	-	-12.0	7.00	+55.0	-	-	10

14	$[Co_3L_3]$	Td	6.767	4.899*	-	-0.67	2.80	-	-	-	11
15	$[(baron^{Me})Co_3]$	Td	7.155	5.319*	-	+5.23	-	-	-	-	12
16	$[Co_3(L^2)(NO_3)_4]\cdot CH_3CN$	Oh	3.31	8.35	98.7–108.4	-4.05	8.00	38.5(2)	-	-	13
17	$[Co_3(L^2)(N_3)_2(NO_3)_2]$	Oh	3.22	8.85	96.2–105.8	+9.74	8.42	46.7(2)	-	-	13
18	$[Co_3(L^2)(NCS)_2(NO_3)_2]\cdot 2CH_3CN$	Oh	3.17	6.97	90.7–106.7	+0.05	8.15	32.5(2)	-	-	13
19	$[(HCDP]_2Co^{II}_3(sil)_2Cl_4(THF)_2]\cdot 4THF$	Oh (central), Td (terminal)	3.029	10.946	97.7(2)	+10.18	7.08	-100, -29	65(2)	$4(2).10^{-10}$	this work

Oh = octahedral, Td = tetrahedral, TBP = trigonal bipyramidal, Sq. Py = square pyramidal, TP = trigonal planar

*The nearest intercluster Co···Co distance is even shorter than the intracluster distance. #In this work, we have used H_{dc} = 2500 Oe. aFor U_{eff} calculated in K, a multiplication factor of k_B = 0.695 cm^{-1} K^{-1} is used to convert in cm^{-1} unit. Abbreviations of the ligands used are detailed as follows:

1. py = pyridine; 2. $N_3O_3H_3L$ = 1,1,1 tris(aminomethyl)ethane + salicylaldehyde; 3. 2-[(pyridine-2-ylimine) methyl]phenol (Hpymp); 4. pya = pridine-2-amine); 5. bca = benzenecarboxylic acid, phen = 1,10-Phenanthroline; 6. bdc = terephthalic acid; 7. H_2dpa = diphenic acid, 1-MeIm = 1-Methylimidazole; 9. OAc_F = CF_3COO^-, BA = benzohydroxamate anion, tmen = *N,N,N′,N′*-tetramethylethylenediamine; 10. L1 = 2,2′,3,3′-tetrahydroxy-benzaldazine, phen =1,10-phenanthroline]; 11, 12. pdz = pyridazine; 13. H_2pytag = 1,2,3-tris[(pyridine-2-ylmethylidene)amino]guanidine; 14. H_2L = *N,N′*-bi(salicylidene)-2,6-pyridinediamine; 15. $baron^{Me}$ = triplesalophen ligand. 16, 17, 18. Mannich–Schiff-base proligand H_2L^2 is obtained by reacting the Mannich base HL^1 with propylenediamine (2:1 molar ratio). HL^1 is obtained from 5-bromo-salicylaldehyde and *N,N,N′*-trimethyl-ethylenediamine; 19. sil = $O(Me_2SiO)_2^{2-}$.

2. Molecular structure and crystal packing of the complex 2

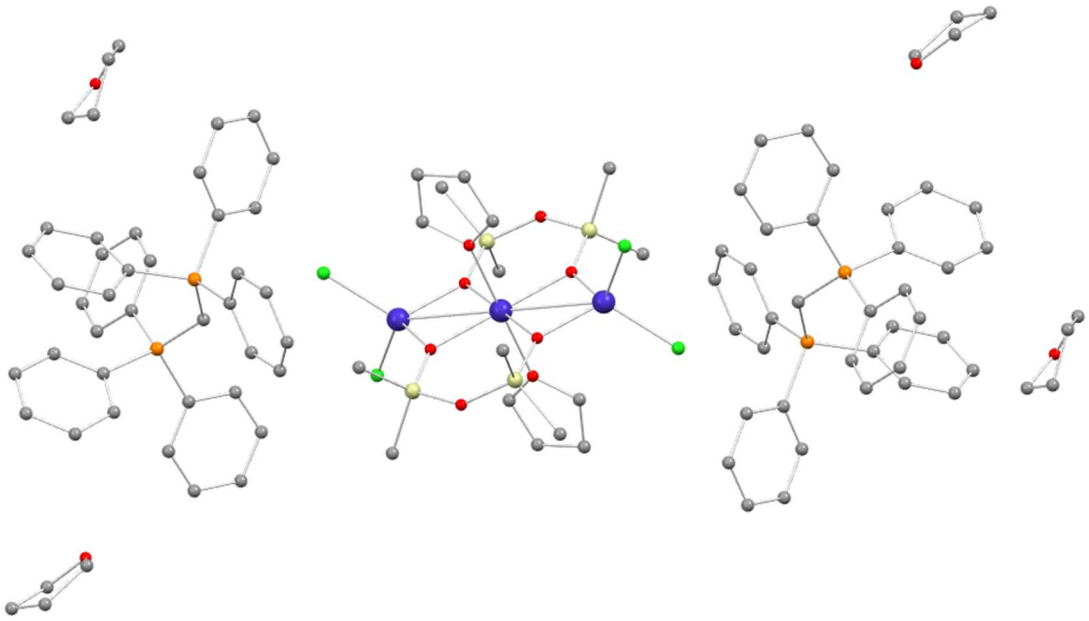

Figure S1. Molecular structure of complex $[(Ph_3P)_2CH]_2[Co^{II}_3(sil)_2Cl_4(THF)_2]\cdot 4THF$ (**2**). sil = $O(Me_2SiO)_2^{2-}$.

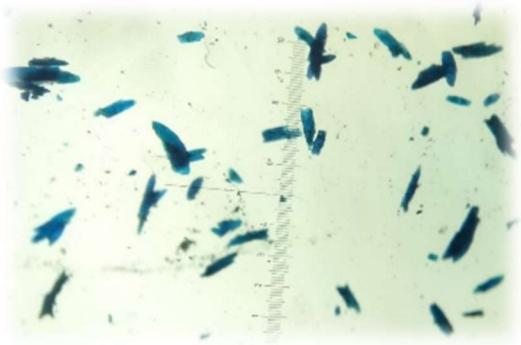

Figure S2. Single crystals picture of complex **2**. All the magnetic measurements are done with these single crystals which were separated mannually.

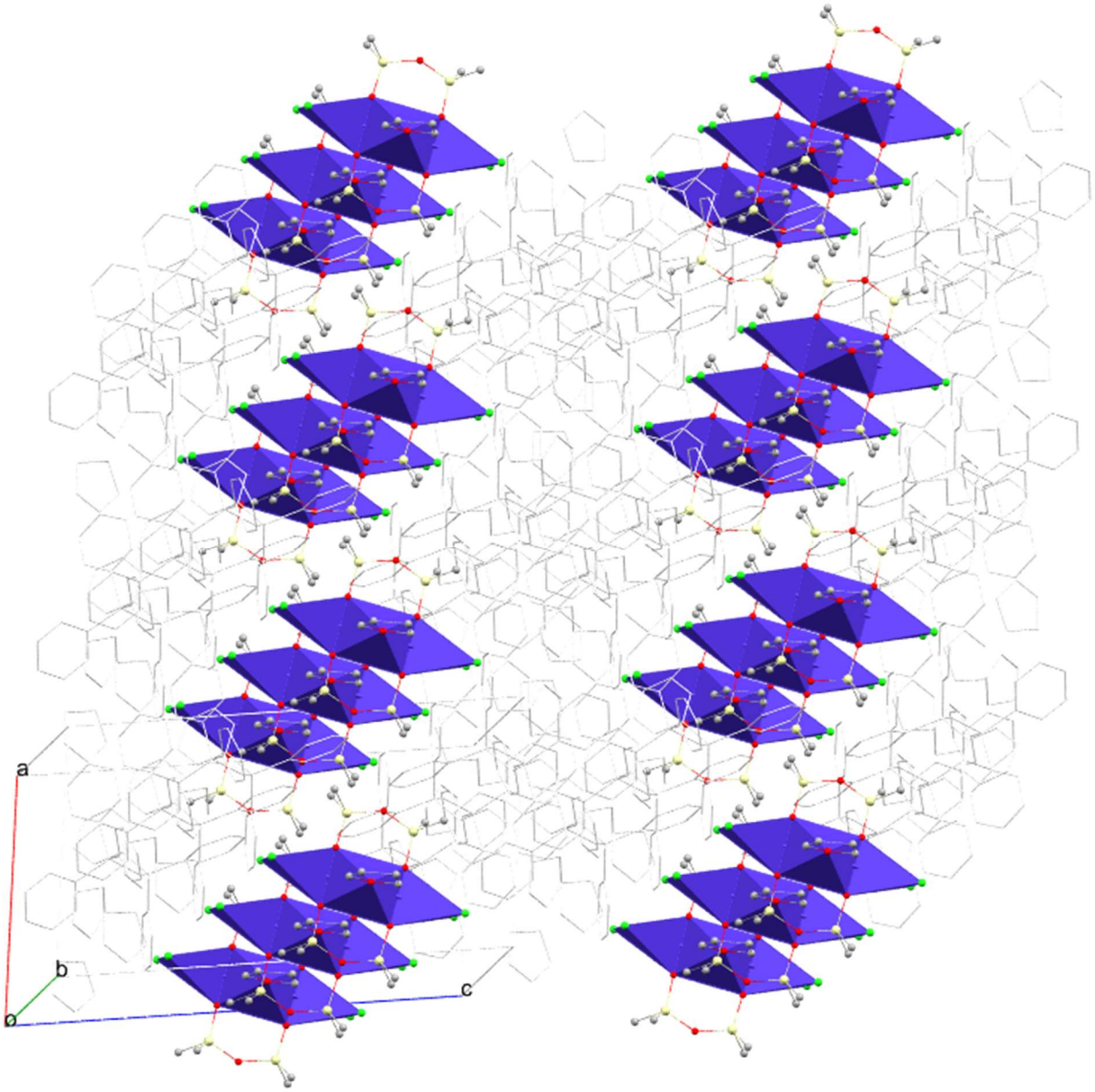

Figure S3. Crystal packing full diagram in **2** viewed opposite to b^* axis. The Co_3 core is highlighted in a polyhedral ball and stick model, keeping carbodiphosphorane (CDP) moieties faded with the wire-frame model.

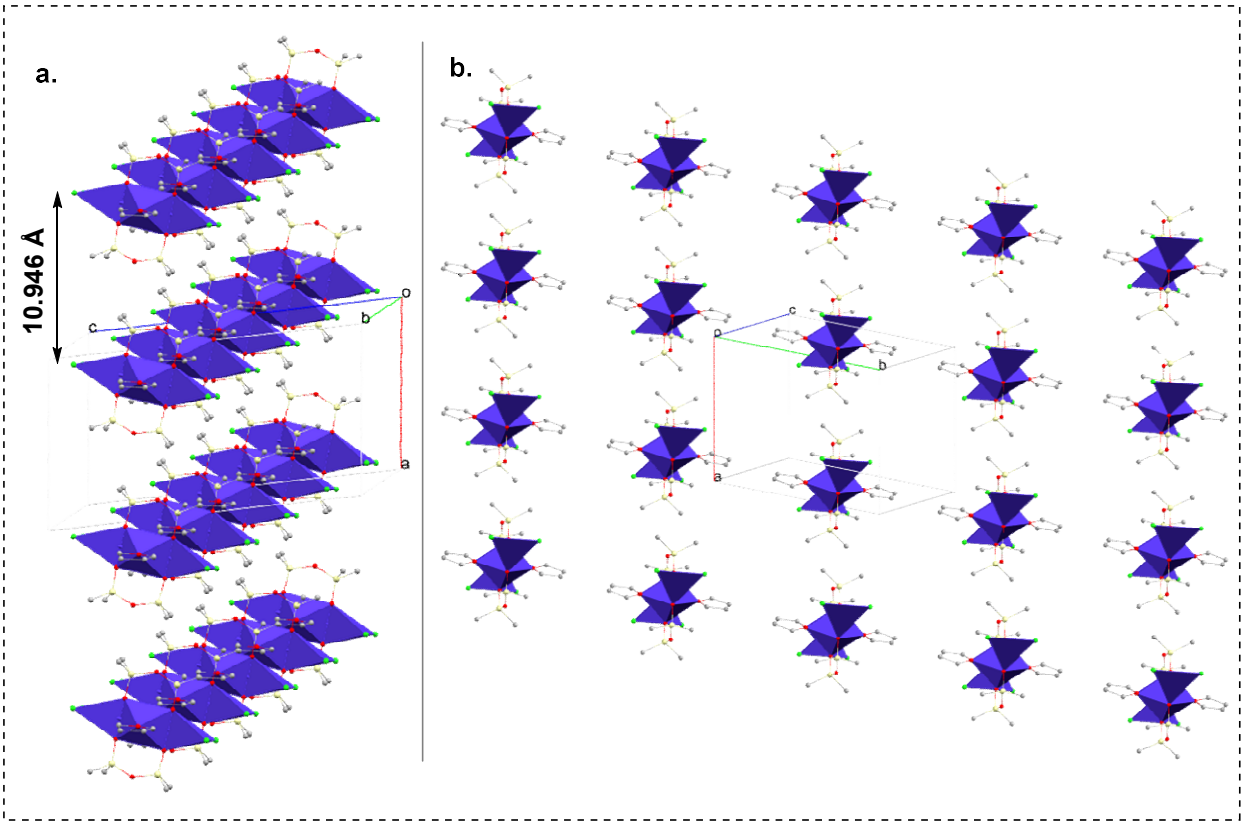

Figure S4. Crystal packing layers of the Co_3 core in **2** viewed in different directions as indicated (*a* in red, *b* in green and *c* in blue). The Co_3 core is represented in a polyhedral ball and stick model. Colours: Co, blue; Si, yellow; Cl, green; O, red; C, grey. The shortest intermolecular distance between Co(1) ions of the two neighboring molecules is 10.946 Å.

3. Crystallographic details

Table S2. Summary of crystallographic parameters and the refinement details of complex **2**.

Identification code	Complex **2**
CCDC Number	**2415240**
Empirical moiety formula	$2(C_{37}H_{30}P_2)$, $C_{16}H_{40}Cl_4Co_3O_8Si_4$, $4(C_4H_8O)$
Sum formula	$C_{106}H_{132}Cl_4Co_3O_{12}P_4Si_4$
Formula weight (g mol^{-1})	2152.95
Temperature (K)	150 (2)
Wavelength (Å)	0.71073
Crystal system	Triclinic
Space group	*P*-1
Unit cell dimensions	*a* = 10.946 (3) Å *b* = 12.514 (3) Å *c* = 19.995 (5) Å α = 81.010 (5)° β = 83.408 (5)° γ = 80.132 (6)°
Volume ($Å^3$)	2654.1 (12)
Z	1
Density (Mg/m^3)	1.347
Absorption coefficient (mm^{-1})	0.728
F (000)	1129
Crystal size (mm^3)	0.250 x 0.200 x 0.150
Theta range for data collection (°)	1.896 to 17.922
Index ranges	$-9 \le h \le 9$, $-10 \le k \le 10$, $-17 \le l \le 17$
Completeness to theta = 17.922°	91.8 %
Refinement method	Full-matrix least-squares on F^2

Extinction coefficient	n/a
R (int)	0.0572
Reflections collected	6119
Independent reflections	3321
Reflections with $I>2\sigma(I)$	2448
Number of restraints	42
parameters	629
Final *R* indices [$I>2\sigma(I)$]	$R_1 = 0.0542$ $wR_2 = 0.1341$
R indices (all data)	$R_1 = 0.0745$ $wR_2 = 0.1479$
GooF	1.008
Largest diff. (Δρ) peak/hole max./min.[e·Å^{-3}]	0.301/-0.283

Here $\boldsymbol{R_1}=\frac{\sum[|\boldsymbol{F_o}|-|\boldsymbol{F_c}|]}{\sum|\boldsymbol{F_o}|}$, $\boldsymbol{wR_2}=\sqrt{\frac{\sum \boldsymbol{w}(\boldsymbol{F_o^2}-\boldsymbol{F_c^2})}{\sum \boldsymbol{w}(\boldsymbol{F_o^2})^2}}$

Table S3. All bond lengths (Å) of complex **2**[a].

C1—P1	1.709 (10)	C36—H36	0.9500
C1—P2	1.717 (10)	C37—H37	0.9500
C2—C3	1.373 (13)	C38—Si1	1.852 (11)
C2—C7	1.379 (13)	C38—H38A	0.9800
C2—P2	1.785 (11)	C38—H38B	0.9800
C3—C4	1.376 (14)	C38—H38C	0.9800
C3—H3	0.9500	C39—Si1	1.795 (12)
C4—C5	1.366 (15)	C39—H39A	0.9800
C4—H4	0.9500	C39—H39B	0.9800

C5—C6	1.382 (15)	C39—H39C	0.9800
C5—H5	0.9500	C40—Si2	1.819 (11)
C6—C7	1.359 (13)	C40—H40A	0.9800
C6—H6	0.9500	C40—H40B	0.9800
C7—H7	0.9500	C40—H40C	0.9800
C8—C9	1.373 (14)	C41—Si2	1.835 (10)
C8—C13	1.383 (13)	C41—H41A	0.9800
C8—P2	1.791 (11)	C41—H41B	0.9800
C9—C10	1.374 (14)	C41—H41C	0.9800
C9—H9	0.9500	C42—O4	1.357 (13)
C10—C11	1.390 (15)	C42—C43	1.460 (15)
C10—H10	0.9500	C42—H42A	0.9900
C11—C12	1.349 (16)	C42—H42B	0.9900
C11—H11	0.9500	C43—C44	1.534 (14)
C12—C13	1.367 (15)	C43—H43A	0.9900
C12—H12	0.9500	C43—H43B	0.9900
C13—H13	0.9500	C44—C45	1.441 (14)
C14—C15	1.362 (13)	C44—H44A	0.9900
C14—C19	1.363 (13)	C44—H44B	0.9900
C14—P2	1.793 (11)	C45—O4	1.368 (13)
C15—C16	1.407 (14)	C45—H45A	0.9900
C15—H15	0.9500	C45—H45B	0.9900
C16—C17	1.349 (15)	C46—O5	1.397 (14)
C16—H16	0.9500	C46—C47	1.465 (17)
C17—C18	1.359 (15)	C46—H46A	0.9900
C17—H17	0.9500	C46—H46B	0.9900
C18—C19	1.369 (14)	C47—C48	1.477 (17)

C18—H18	0.9500	C47—H47A	0.9900
C19—H19	0.9500	C47—H47B	0.9900
C20—C21	1.357 (14)	C48—C49	1.451 (17)
C20—C25	1.366 (13)	C48—H48A	0.9900
C20—P1	1.789 (11)	C48—H48B	0.9900
C21—C22	1.389 (15)	C49—O5	1.400 (14)
C21—H21	0.9500	C49—H49A	0.9900
C22—C23	1.367 (16)	C49—H49B	0.9900
C22—H22	0.9500	C50—O6	1.374 (14)
C23—C24	1.356 (15)	C50—C51	1.534 (16)
C23—H23	0.9500	C50—H50A	0.9900
C24—C25	1.387 (14)	C50—H50B	0.9900
C24—H24	0.9500	C51—C52	1.483 (17)
C25—H25	0.9500	C51—H51A	0.9900
C26—C31	1.376 (13)	C51—H51B	0.9900
C26—C27	1.394 (13)	C52—C53	1.503 (17)
C26—P1	1.801 (11)	C52—H52A	0.9900
C27—C28	1.373 (13)	C52—H52B	0.9900
C27—H27	0.9500	C53—O6	1.414 (13)
C28—C29	1.360 (13)	C53—H53A	0.9900
C28—H28	0.9500	C53—H53B	0.9900
C29—C30	1.370 (13)	Cl1—Co2	2.278 (3)
C29—H29	0.9500	Cl2—Co2	2.291 (3)
C30—C31	1.378 (13)	Co1—O3	2.061 (6)
C30—H30	0.9500	Co1—O3^{i}	2.061 (6)
C31—H31	0.9500	Co1—O1	2.069 (6)
C32—C33	1.376 (13)	Co1—O1^{i}	2.069 (6)

C32—C37	1.401 (13)	Co1—O4^{i}	2.200 (7)
C32—P1	1.794 (11)	Co1—O4	2.200 (7)
C33—C34	1.364 (15)	Co2—O1	1.952 (6)
C33—H33	0.9500	Co2—O3^{i}	1.959 (6)
C34—C35	1.380 (15)	Si1—O1	1.601 (6)
C34—H34	0.9500	Si1—O2	1.625 (7)
C35—C36	1.379 (14)	Si2—O3	1.615 (6)
C35—H35	0.9500	Si2—O2	1.623 (7)
C36—C37	1.358 (13)		

[a] Symmetry transformations used to generate equivalent atoms: (^{i}) -x+2, -y+1, -z+1.

Table S4. All bond angles (°) of complex **2**[a].

P1—C1—P2	127.8 (6)	H41A—C41—H41C	109.5
C3—C2—C7	118.9 (10)	H41B—C41—H41C	109.5
C3—C2—P2	118.7 (10)	O4—C42—C43	111.3 (11)
C7—C2—P2	122.4 (10)	O4—C42—H42A	109.4
C2—C3—C4	120.3 (10)	C43—C42—H42A	109.4
C2—C3—H3	119.9	O4—C42—H42B	109.4
C4—C3—H3	119.9	C43—C42—H42B	109.4
C5—C4—C3	120.6 (11)	H42A—C42—H42B	108.0
C5—C4—H4	119.7	C42—C43—C44	104.2 (9)
C3—C4—H4	119.7	C42—C43—H43A	110.9
C4—C5—C6	119.0 (11)	C44—C43—H43A	110.9
C4—C5—H5	120.5	C42—C43—H43B	110.9
C6—C5—H5	120.5	C44—C43—H43B	110.9
C7—C6—C5	120.4 (10)	H43A—C43—H43B	108.9
C7—C6—H6	119.8	C45—C44—C43	102.1 (9)

C5—C6—H6	119.8	C45—C44—H44A	111.3
C6—C7—C2	120.8 (10)	C43—C44—H44A	111.3
C6—C7—H7	119.6	C45—C44—H44B	111.3
C2—C7—H7	119.6	C43—C44—H44B	111.3
C9—C8—C13	119.2 (9)	H44A—C44—H44B	109.2
C9—C8—P2	122.4 (10)	O4—C45—C44	113.7 (10)
C13—C8—P2	118.4 (10)	O4—C45—H45A	108.8
C8—C9—C10	121.2 (11)	C44—C45—H45A	108.8
C8—C9—H9	119.4	O4—C45—H45B	108.8
C10—C9—H9	119.4	C44—C45—H45B	108.8
C9—C10—C11	118.9 (11)	H45A—C45—H45B	107.7
C9—C10—H10	120.5	O5—C46—C47	105.5 (12)
C11—C10—H10	120.5	O5—C46—H46A	110.6
C12—C11—C10	119.4 (12)	C47—C46—H46A	110.6
C12—C11—H11	120.3	O5—C46—H46B	110.6
C10—C11—H11	120.3	C47—C46—H46B	110.6
C11—C12—C13	122.1 (12)	H46A—C46—H46B	108.8
C11—C12—H12	119.0	C46—C47—C48	102.1 (11)
C13—C12—H12	119.0	C46—C47—H47A	111.4
C12—C13—C8	119.2 (11)	C48—C47—H47A	111.4
C12—C13—H13	120.4	C46—C47—H47B	111.4
C8—C13—H13	120.4	C48—C47—H47B	111.4
C15—C14—C19	120.4 (10)	H47A—C47—H47B	109.2
C15—C14—P2	120.6 (10)	C49—C48—C47	103.3 (12)
C19—C14—P2	119.1 (10)	C49—C48—H48A	111.1
C14—C15—C16	119.0 (11)	C47—C48—H48A	111.1
C14—C15—H15	120.5	C49—C48—H48B	111.1

C16—C15—H15	120.5	C47—C48—H48B	111.1
C17—C16—C15	119.2 (12)	H48A—C48—H48B	109.1
C17—C16—H16	120.4	O5—C49—C48	108.5 (12)
C15—C16—H16	120.4	O5—C49—H49A	110.0
C16—C17—C18	121.6 (12)	C48—C49—H49A	110.0
C16—C17—H17	119.2	O5—C49—H49B	110.0
C18—C17—H17	119.2	C48—C49—H49B	110.0
C17—C18—C19	119.3 (11)	H49A—C49—H49B	108.4
C17—C18—H18	120.3	O6—C50—C51	108.6 (12)
C19—C18—H18	120.3	O6—C50—H50A	110.0
C14—C19—C18	120.5 (11)	C51—C50—H50A	110.0
C14—C19—H19	119.8	O6—C50—H50B	110.0
C18—C19—H19	119.8	C51—C50—H50B	110.0
C21—C20—C25	119.1 (10)	H50A—C50—H50B	108.4
C21—C20—P1	116.4 (11)	C52—C51—C50	102.7 (11)
C25—C20—P1	124.3 (11)	C52—C51—H51A	111.2
C20—C21—C22	121.0 (12)	C50—C51—H51A	111.2
C20—C21—H21	119.5	C52—C51—H51B	111.2
C22—C21—H21	119.5	C50—C51—H51B	111.2
C23—C22—C21	118.8 (11)	H51A—C51—H51B	109.1
C23—C22—H22	120.6	C51—C52—C53	106.4 (12)
C21—C22—H22	120.6	C51—C52—H52A	110.5
C24—C23—C22	120.9 (12)	C53—C52—H52A	110.5
C24—C23—H23	119.6	C51—C52—H52B	110.5
C22—C23—H23	119.6	C53—C52—H52B	110.5
C23—C24—C25	119.4 (12)	H52A—C52—H52B	108.6
C23—C24—H24	120.3	O6—C53—C52	107.2 (11)

C25—C24—H24	120.3	O6—C53—H53A	110.3
C20—C25—C24	120.6 (10)	C52—C53—H53A	110.3
C20—C25—H25	119.7	O6—C53—H53B	110.3
C24—C25—H25	119.7	C52—C53—H53B	110.3
C31—C26—C27	117.7 (10)	H53A—C53—H53B	108.5
C31—C26—P1	123.2 (10)	O3—Co1—O3^{i}	180.00 (12)
C27—C26—P1	119.1 (10)	O3—Co1—O1	100.5 (2)
C28—C27—C26	120.7 (10)	O3^{i}—Co1—O1	79.5 (2)
C28—C27—H27	119.7	O3—Co1—O1^{i}	79.5 (2)
C26—C27—H27	119.7	O3^{i}—Co1—O1^{i}	100.5 (2)
C29—C28—C27	120.2 (10)	O1—Co1—O1^{i}	180.0
C29—C28—H28	119.9	O3—Co1—O4^{i}	90.3 (3)
C27—C28—H28	119.9	O3^{i}—Co1—O4^{i}	89.7 (3)
C28—C29—C30	120.5 (10)	O1—Co1—O4^{i}	89.5 (2)
C28—C29—H29	119.8	O1^{i}—Co1—O4^{i}	90.5 (2)
C30—C29—H29	119.8	O3—Co1—O4	89.7 (3)
C29—C30—C31	119.3 (10)	O3^{i}—Co1—O4	90.3 (3)
C29—C30—H30	120.3	O1—Co1—O4	90.5 (2)
C31—C30—H30	120.3	O1^{i}—Co1—O4	89.5 (2)
C26—C31—C30	121.6 (10)	O4^{i}—Co1—O4	180.0
C26—C31—H31	119.2	O1—Co2—O3^{i}	85.0 (2)
C30—C31—H31	119.2	O1—Co2—Cl1	117.21 (19)
C33—C32—C37	119.3 (9)	O3^{i}—Co2—Cl1	114.61 (18)
C33—C32—P1	118.7 (10)	O1—Co2—Cl2	115.18 (19)
C37—C32—P1	121.8 (10)	O3^{i}—Co2—Cl2	120.31 (18)
C34—C33—C32	119.3 (11)	Cl1—Co2—Cl2	104.55 (11)
C34—C33—H33	120.4	C1—P1—C20	113.5 (5)

C32—C33—H33	120.4	C1—P1—C32	115.9 (6)
C33—C34—C35	121.6 (12)	C20—P1—C32	108.0 (6)
C33—C34—H34	119.2	C1—P1—C26	106.4 (5)
C35—C34—H34	119.2	C20—P1—C26	109.6 (6)
C36—C35—C34	119.2 (11)	C32—P1—C26	102.8 (5)
C36—C35—H35	120.4	C1—P2—C2	112.2 (5)
C34—C35—H35	120.4	C1—P2—C8	110.5 (6)
C37—C36—C35	119.9 (10)	C2—P2—C8	105.8 (5)
C37—C36—H36	120.1	C1—P2—C14	115.5 (5)
C35—C36—H36	120.1	C2—P2—C14	104.5 (6)
C36—C37—C32	120.7 (10)	C8—P2—C14	107.6 (6)
C36—C37—H37	119.7	O1—Si1—O2	109.8 (3)
C32—C37—H37	119.7	O1—Si1—C39	111.6 (5)
Si1—C38—H38A	109.5	O2—Si1—C39	109.5 (6)
Si1—C38—H38B	109.5	O1—Si1—C38	111.6 (5)
H38A—C38—H38B	109.5	O2—Si1—C38	106.4 (5)
Si1—C38—H38C	109.5	C39—Si1—C38	107.8 (7)
H38A—C38—H38C	109.5	O3—Si2—O2	109.8 (3)
H38B—C38—H38C	109.5	O3—Si2—C40	111.1 (4)
Si1—C39—H39A	109.5	O2—Si2—C40	106.5 (5)
Si1—C39—H39B	109.5	O3—Si2—C41	111.8 (4)
H39A—C39—H39B	109.5	O2—Si2—C41	108.7 (5)
Si1—C39—H39C	109.5	C40—Si2—C41	108.8 (5)
H39A—C39—H39C	109.5	Si1—O1—Co2	134.4 (4)
H39B—C39—H39C	109.5	Si1—O1—Co1	127.9 (3)
Si2—C40—H40A	109.5	Co2—O1—Co1	97.7 (2)
Si2—C40—H40B	109.5	Si2—O2—Si1	140.9 (4)

H40A—C40—H40B	109.5	Si2—O3—Co2^{i}	134.6 (4)
Si2—C40—H40C	109.5	Si2—O3—Co1	127.5 (3)
H40A—C40—H40C	109.5	Co2^{i}—O3—Co1	97.8 (2)
H40B—C40—H40C	109.5	C42—O4—C45	107.6 (9)
Si2—C41—H41A	109.5	C42—O4—Co1	126.2 (7)
Si2—C41—H41B	109.5	C45—O4—Co1	126.2 (7)
H41A—C41—H41B	109.5	C46—O5—C49	107.7 (11)
Si2—C41—H41C	109.5	C50—O6—C53	111.0 (10)

[a] Symmetry transformations used to generate equivalent atoms: (^{i}) -x+2, -y+1, -z+1.

4. UV-Visible spectrum

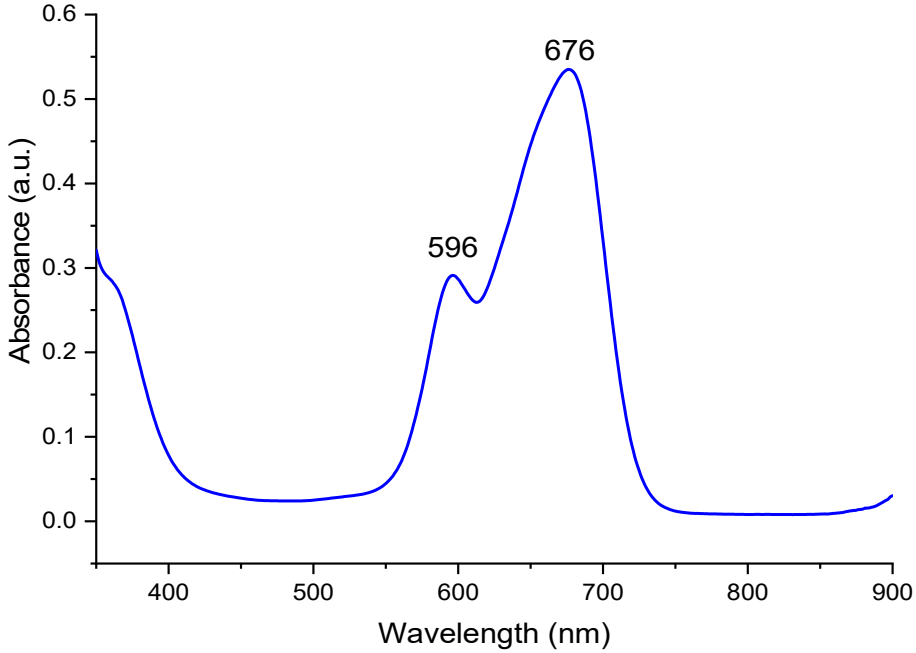

Figure S5. UV-Visible spectrum (blue) of complex **2** from 350 nm to 900 nm. **2** in THF is blue coloured [λ_{max} (nm): 596, 676].

5. IR spectrum

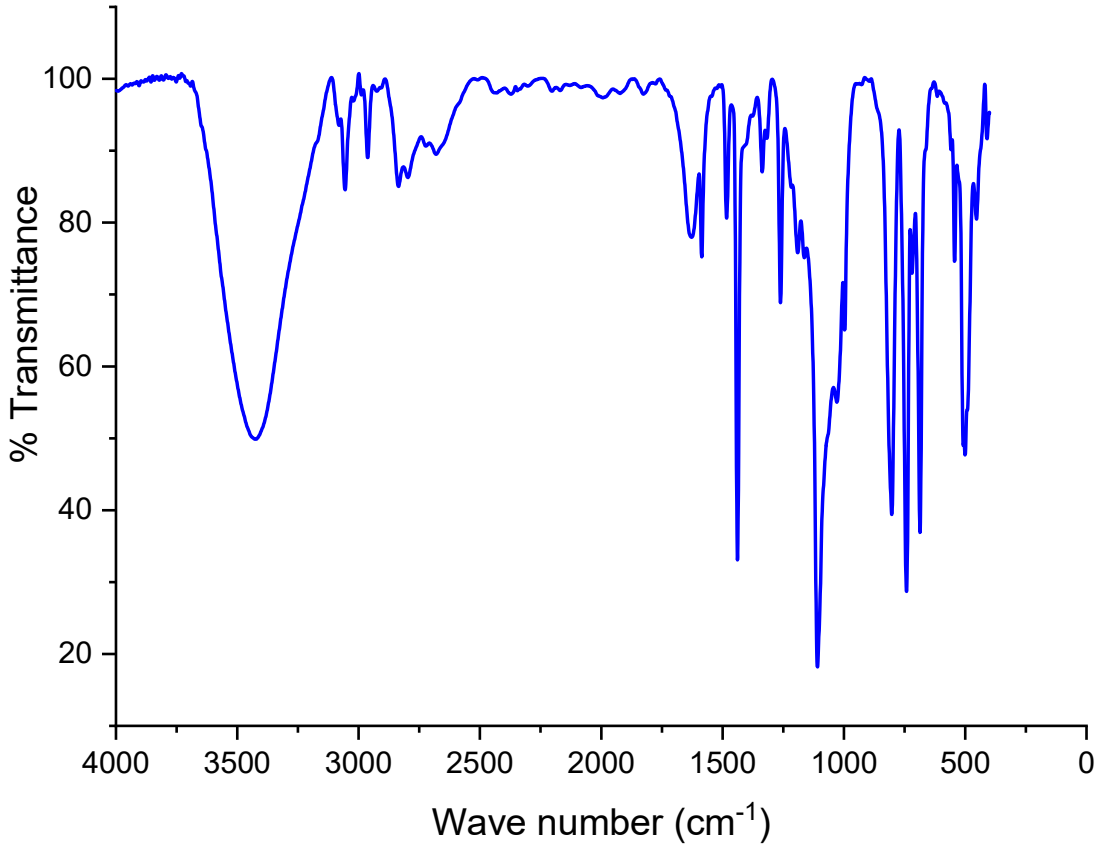

Figure S6. IR spectrum of complex **2**. Stretching frequency (υ, cm^{-1}): 3055, 2960, 2839, 2799, 2725, 2680, 1625, 1588, 1487, 1440, 1264, 1187, 1163, 1109, 1025, 994, 805, 745, 684, 502.

6. ESI HRMS analysis

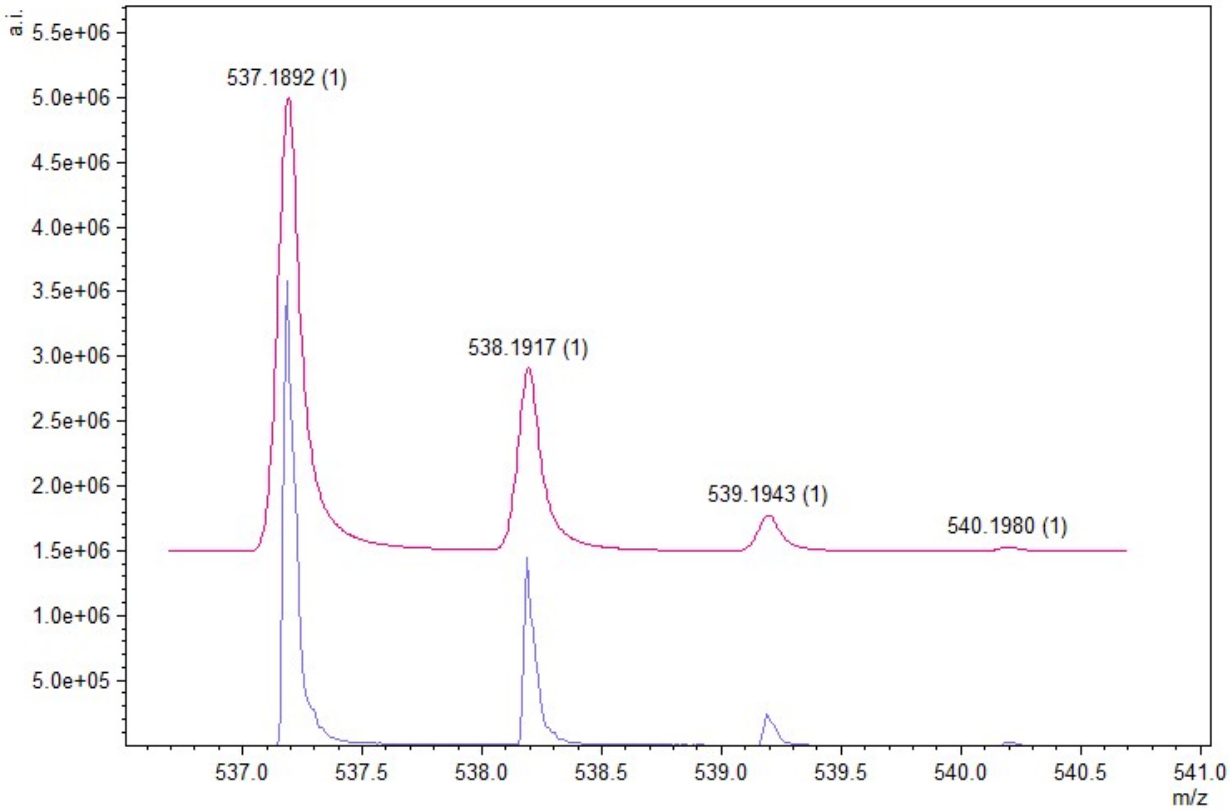

Figure S7. Experimental (blue) and simulated (red) ESI HRMS spectra in positive mode $[M+H]^+$ of **2** in acetonitrile solvent gave fragment ion peaks for CDP (m/z = 536) moiety only.

7. EPR analysis

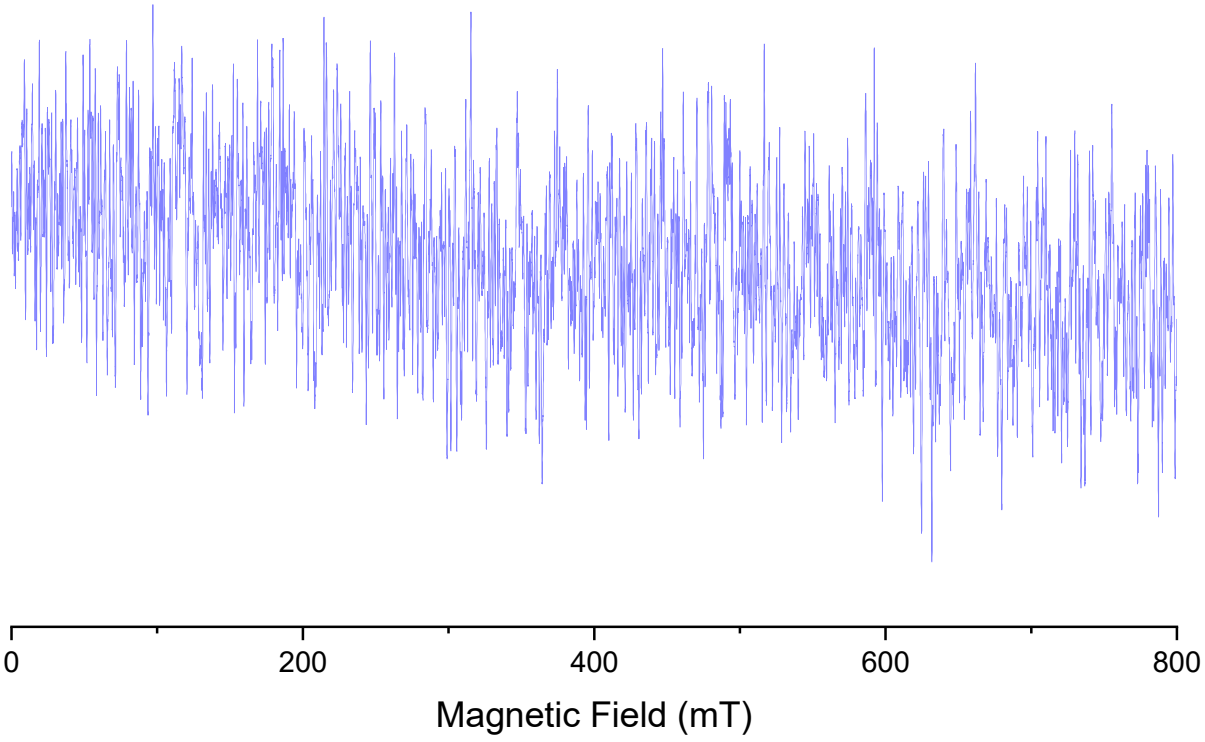

Figure S8. X-band EPR spectrum of **2** at room temperature in DMSO medium at the frequency of 9.45 GHz. The spectrum is silent in this region.

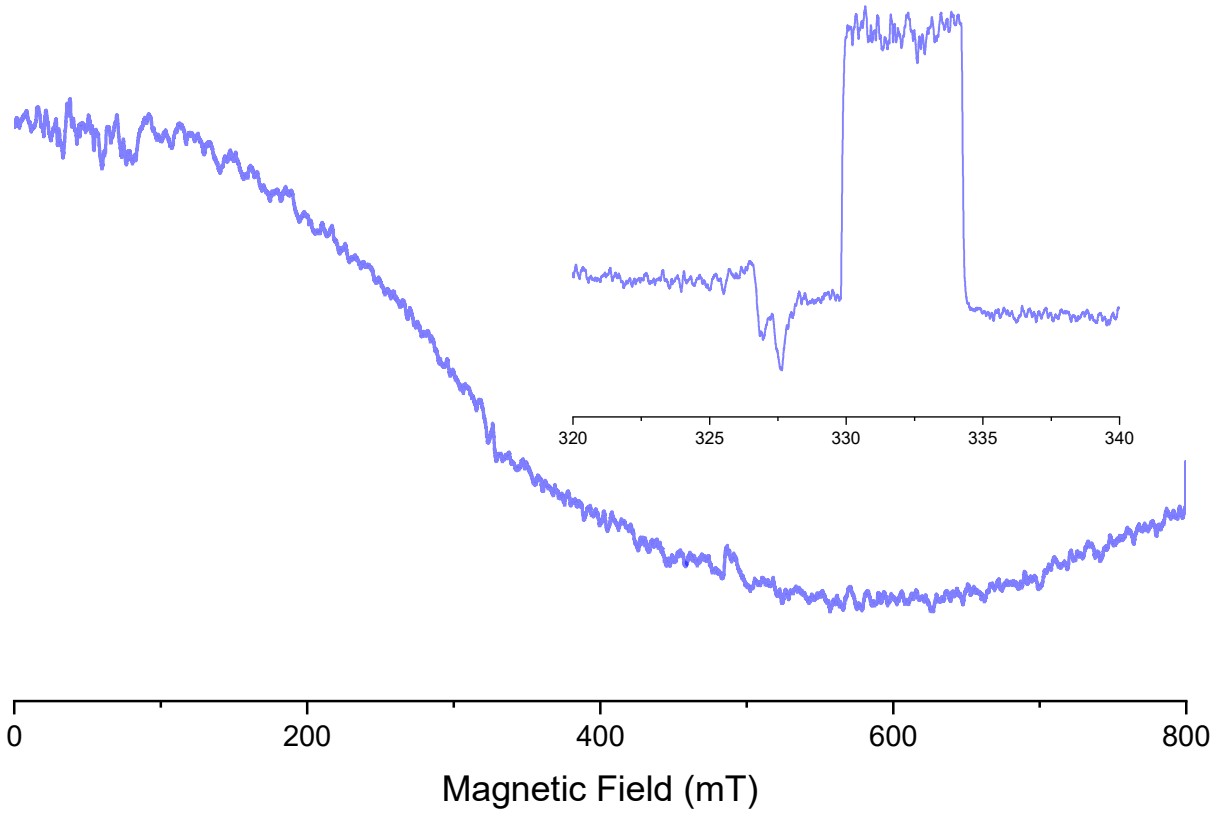

Figure S9. X-band EPR spectrum (inset is the bloom up view from 320 mT to 340 mT) of **2** at 77 K temperature in DMSO medium at the frequency of 9.16 GHz. The spectrum is silent in this region. The weak signals at 323 mT and 327 mT are due to the impurity (confirmed from the blank tube spectrum). The surge at 330 mT is due to the dissolved molecular dioxygen in liquid N_2 used for 77 K temperature.

8. PXRD analysis

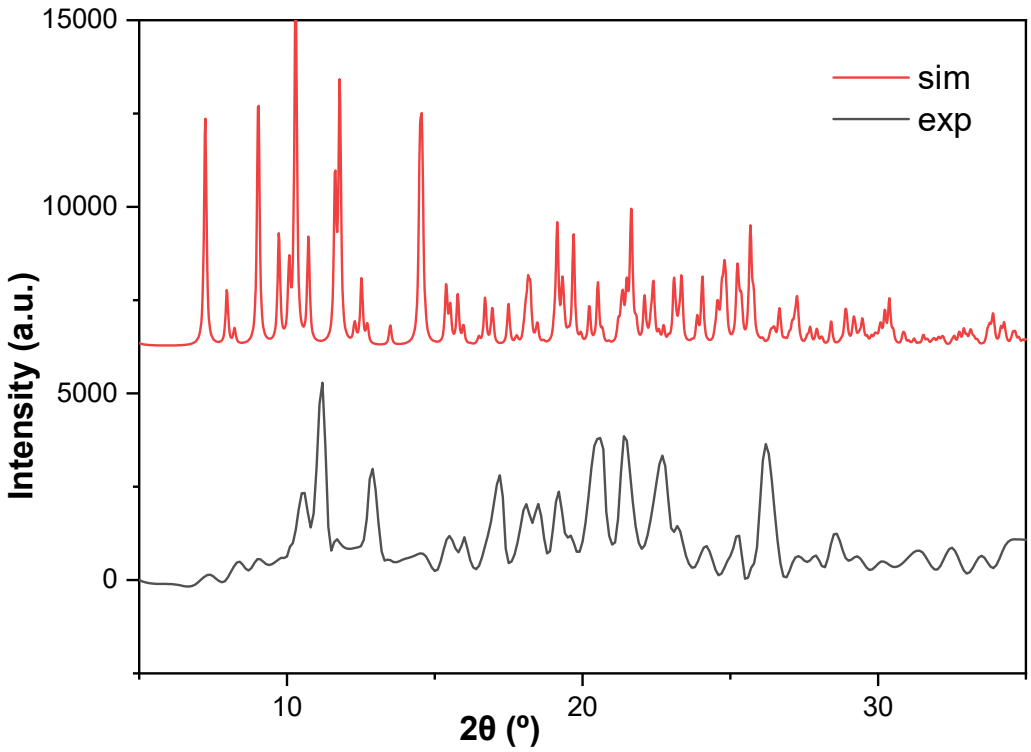

Figure S10. The experimental PXRD pattern (black) and simulated PXRD pattern from single-crystal X-ray diffraction (red) for complex **2**. The small differences between both diffractograms might be due to the loss of coordinated THF solvent molecules.

9. TGA analysis

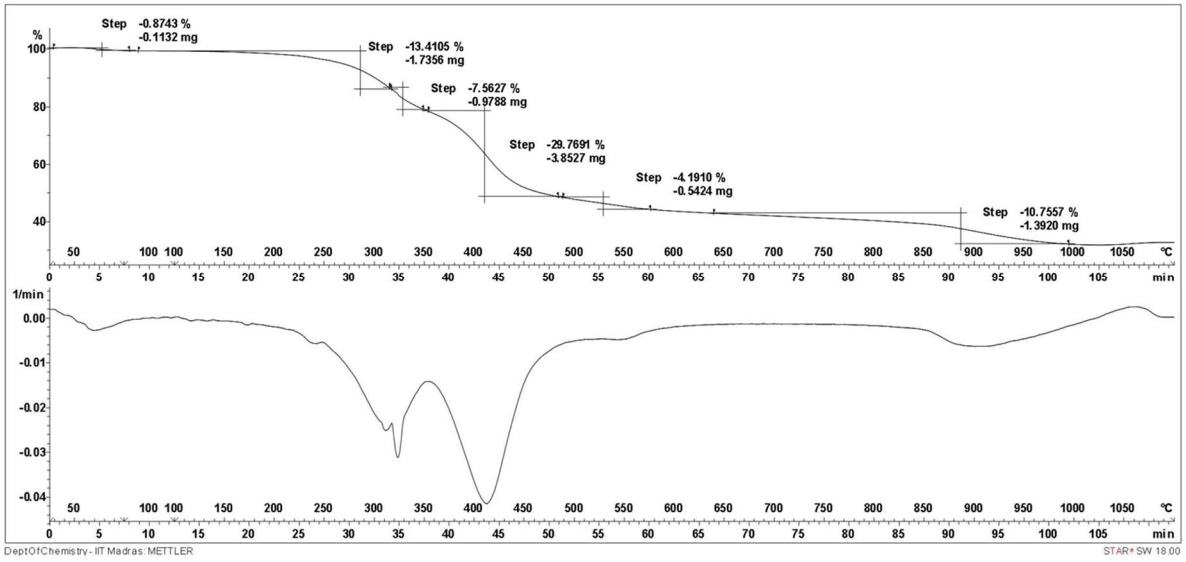

Figure S11. Thermogravimetric analysis (TGA) for Co^{II}_3-complex from 30 °C to 1100 °C showed decomposition of the complex at around 250 °C. Lattice THF molecules were lost prior to the TGA measurements. The coordinated THF molecules on the central Co^{II} ion are lost above 160 °C.

10. NMR Spectra

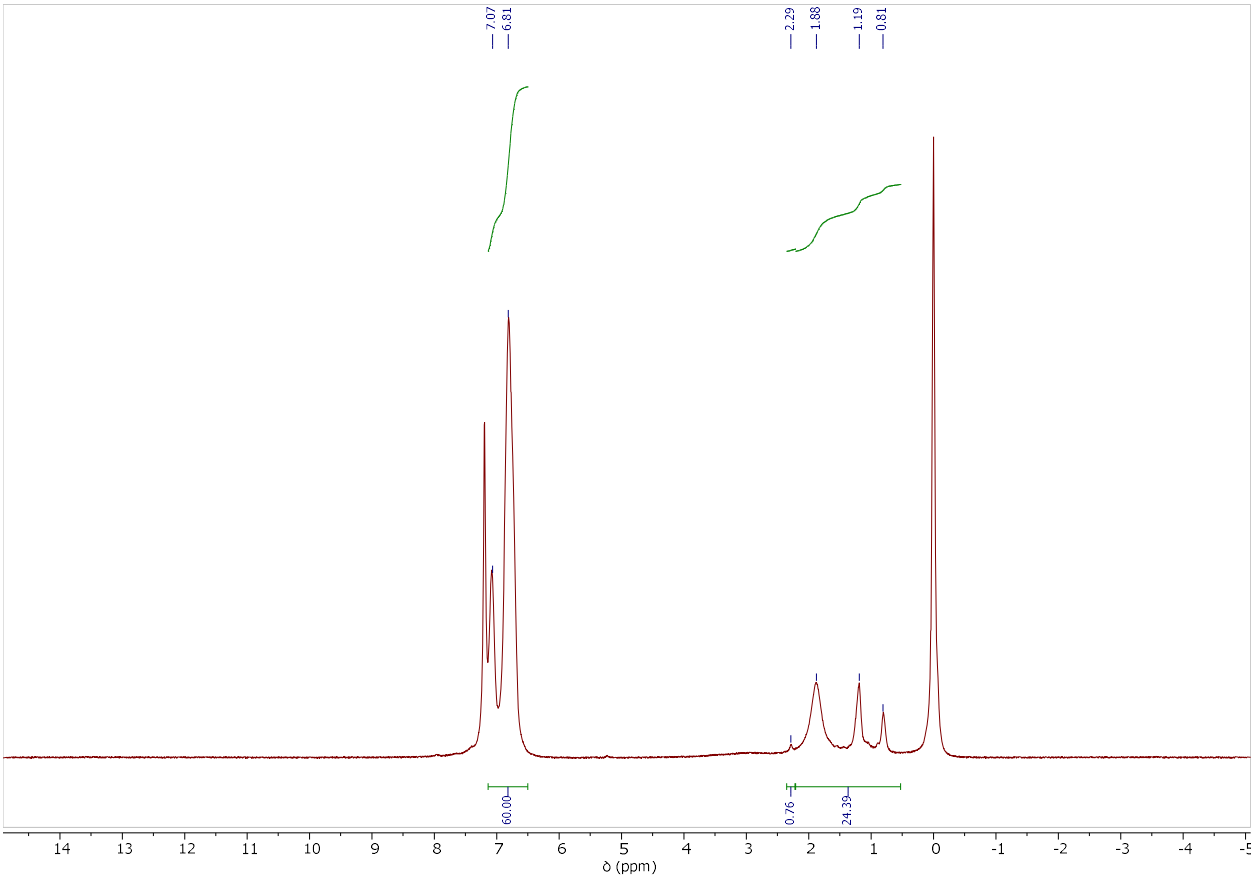

Figure S12. ^{1}H NMR spectrum of **2** (δ in ppm: 0.91, 1.19, 1.88 for the CH_3; 2.29 for CH^+; and 6.81, 7.07 for the aromatic H) in $CDCl_3$ solvent (sky blue-coloured solution) at room temperature. The resonance near zero ppm is due to the reference (TMS; trimethylsilane).

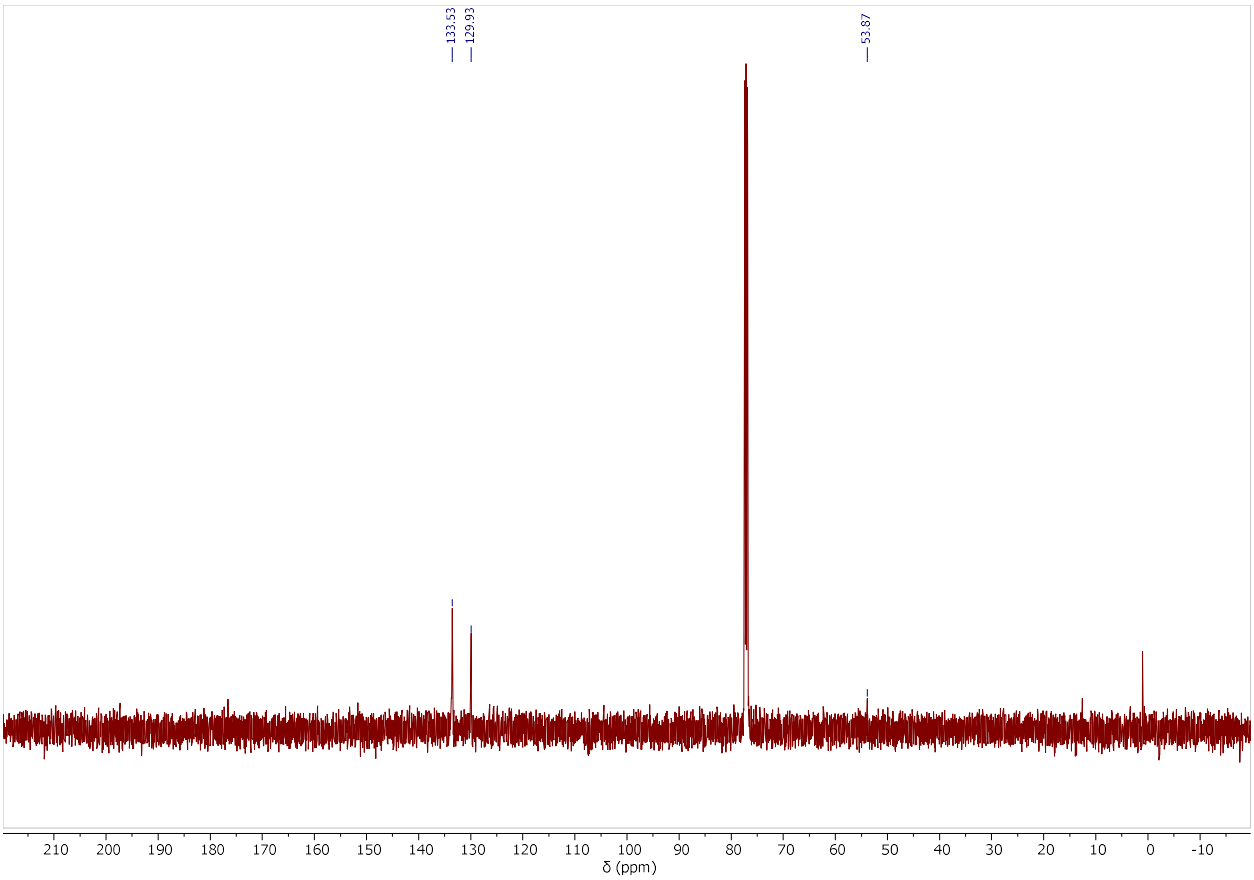

Figure S13. ^{13}C NMR spectrum of **2** (δ in ppm: 129.93, 133.53 for aromatic C; 53.87 for aliphatic C) in $CDCl_3$ solvent (sky blue-coloured solution) at room temperature.

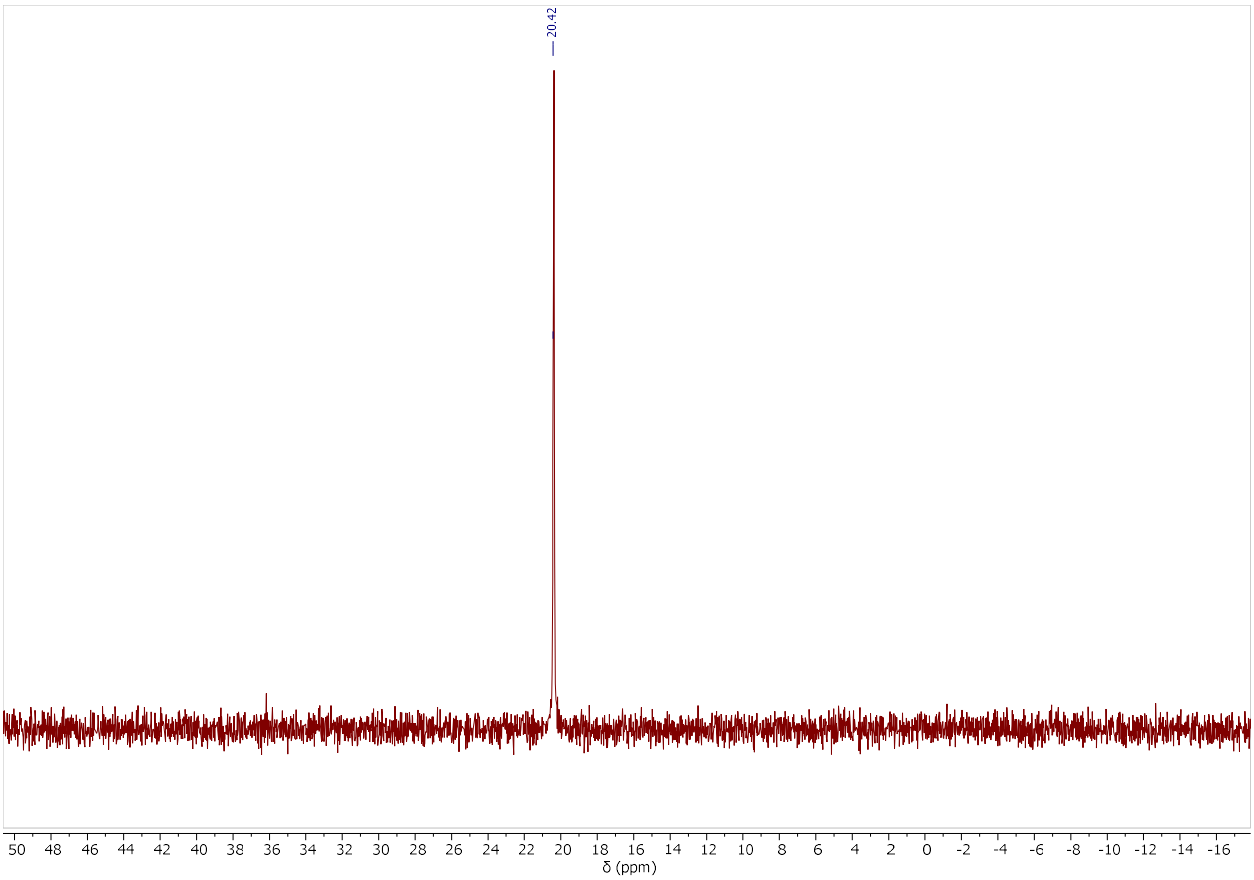

Figure S14. ^{31}P NMR spectrum of sky blue-coloured solution of **2** (δ in ppm: 20.42, corresponding to the ^{31}P nuclei of $(Ph_3P)_2CH^+$ cation in $CDCl_3$ solvent at room temperature.

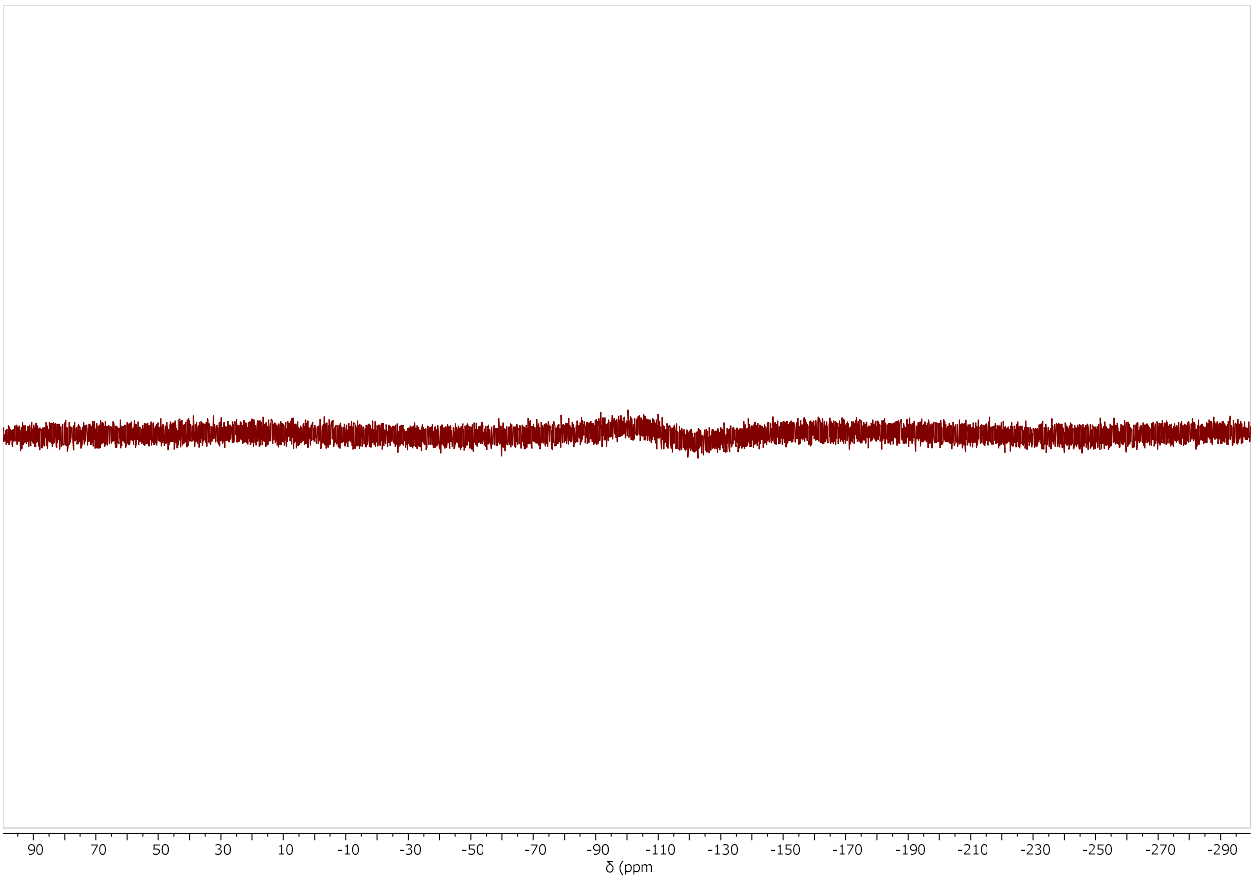

Figure S15. ^{29}Si NMR spectrum of **2** in $CDCl_3$ solvent (sky blue-coloured solution) at room temperature. However, there was no detectable signal instead of a broad hump that came in ^{29}Si NMR at δ (ppm): -110, which is due to the background Si present in the NMR tube.

11. Equations used to relate susceptibility with Curie constant and paramagnetic moment

The magnetic molar susceptibility (χ_m) given by Curie's law is defined as–

$$\chi_m=\frac{\mu_0 N_A \mu_{eff}^2 \mu_B^2}{3k_B T}=\frac{C}{T} \qquad \textbf{eq. S1}$$

Where μ_B=9.274×10^{-24} J T^{-1} = Bohr magneton that corresponds to the magnetic moment of a 1s electron in hydrogen, μ_0=1.256×10^{-6} N A^{-2} = vacuum permeability, N_A=6.023×10^{23} = Avogadro's constant; k_B=1.38×10^{-23} = Boltzmann's constant, μ_{eff}= effective magnetic moment in Bohr magneton, T= temperature in K and C = Curie constant.

Hence, $\chi_m T$ is independent of temperature, and this can be related to the effective magnetic moment (μ_{eff}). Therefore, by rearranging **eq. S1**, one has–

$$\mu_{eff}=(3k_B/\mu_0 N_A \mu_B^2)^{1/2}\sqrt{\chi_m T} \qquad \textbf{eq. S2}$$

So that, $\mu_{eff}=800\sqrt{\chi_m T}$ (χ_m is in m^3 mol^{-1}, in SI unit) **eq. S4**

$\mu_{eff}=\sqrt{8\chi_m T}$ (χ_m is in cm^3 mol^{-1}, in cgs unit) **eq. S5**

Where μ_{eff} is measured in Bohr magnetons (μ_B) per formula unit.

12.Curie-Weiss fit to molar magnetic susceptibility

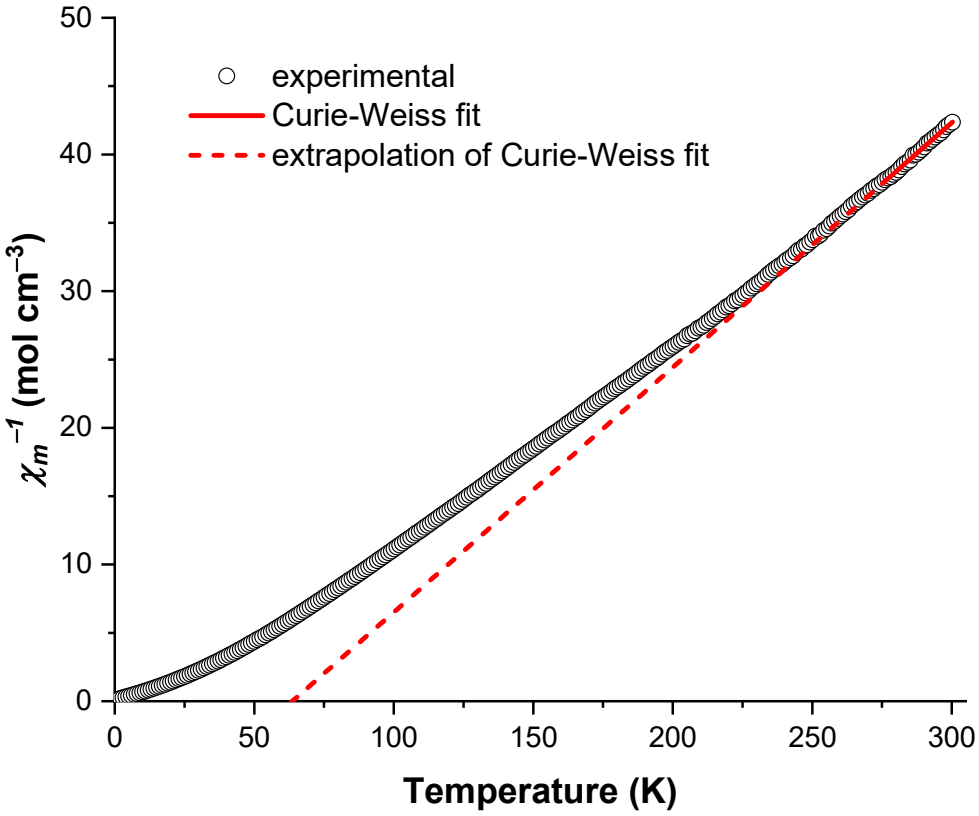

Figure S16. Measured inverse susceptibility χ_m^{-1} vs temperature (T) of complex **2** obtained at 2500 Oe (open circles). A Curie-Weiss fit (**eq. 2**) has been performed to a short temperature region from 275 K to 300 K (solid line). The dashed line is an extrapolation of the Curie-Weiss fit to lower temperature.

13.Diamagnetic susceptibility corrections

Total diamagnetic susceptibility corrections (χ_D) = Total atomic ($\sum_i \chi_{Di}$) + bond ($\sum_i \lambda_i$) contribution.

$\therefore \chi_D = \sum_i \chi_{Di} + \sum_i \lambda_i$

To prevent the loss of the solvent of crystallization in **2**, the sample was kept a little wet, and the molecular weight of **2** was modified to 2441 considering a total 8THF solvent of crystallization. Now molecular formula: $(HCDP)_2[Co^{II}_3(sil)_2Cl_4(THF)_2].8THF$ where HCDP = $H^+C(PPh_3)_2$, sil = $O(Me_2SiO)_2^{2-}$ *i.e.* **2 ($C_{37}H_{31}P_2$) + ($C_8H_{24}Cl_4Co_3O_6Si_4$) + 10 (C_4H_8O).**

Table S5. Total diamagnetic susceptibility corrections for complex **2.**

Atomic diamagnetic contribution to magnetic susceptibility	$\left(\sum \chi_{Di}\right)_1 = 2 \times [1 \times \chi_{C(open)} + 36 \times \chi_{C(ring)} + 31 \times \chi_H + 2 \times \chi_P]$ $= 2 \times [1 \times (6.00) + 36 \times (6.24) + 31 \times (2.93) + 2 \times (26.3)] \times (-10^{-6}\ emu.mol^{-1})$ $= -748.14 \times 10^{-6}\ emu.mol^{-1}$ $\left(\sum \chi_{Di}\right)_2 = 8 \times \chi_{C(open)} + 24 \times \chi_H + 4 \times \chi_{Cl} + 3 \times \chi_{Co} + 6 \times \chi_O + 4 \times \chi_{Si}$ $= [8 \times (6.00) + 24 \times (2.93) + 4 \times (20.1) + 3 \times (12) + 6 \times (4.6) + 4 \times (13)] \times (-10^{-6}\ emu.mol^{-1})$ $= -314.32 \times 10^{-6}\ emu.mol^{-1}$ $\left(\sum \chi_{Di}\right)_3 = 10 \times [4 \times \chi_{C(ring)} + 8 \times \chi_H + 1 \times \chi_O]$ $= 10 \times [4 \times (6.24) + 8 \times (2.93) + 1 \times (4.6)] \times (-10^{-6}\ emu.mol^{-1})$ $= -530.00 \times 10^{-6}\ emu.mol^{-1}$ Now, $(\sum_i \chi_{Di})_{total} = (\sum \chi_{Di})_1 + (\sum \chi_{Di})_2 + (\sum \chi_{Di})_3$ $= (748.14 + 314.32 + 530.00) \times (-10^{-6}\ emu.mol^{-1})$ $= -1592.46 \times 10^{-6}\ emu.mol^{-1}$
Bond diamagnetic contribution to magnetic susceptibility	$\sum_i \lambda_i = (\lambda_i)_{10(THF)} + (\lambda_I)_{4(PPh_3)}$ $= (\lambda_i)_{10(furan)} + (\lambda_i)_{12(Benzene)}$ $= [10 \times (2.5) + 12 \times (1.4)] \times (-10^{-6}\ emu.mol^{-1})$ $= -41.8 \times 10^{-6}\ emu.mol^{-1}$

$\therefore \chi_D = \sum_i \chi_{Di} + \sum_i \lambda_i$

$= (1380.46 + 31.8) \times (-10^{-6}\ emu.mol^{-1})$

$= -1634.26 \times 10^{-6}\ emu.mol^{-1}$

14. Estimation of low temperature relaxation times from time evolution of dc magnetization for complex 2

The available sample mass of 3.3 mg of complex **2** was measured with the same setup as used for the dc field scans and susceptibility measurements (see experimental section in the main text). Coming from room temperature, the sample was held at 10 K and a field of -1 T (-10 kOe) was set. Then the sample was cooled down to 2 K and a continuous VSM dc magnetization measurement (with averaging time of 5 seconds) was started to track the evolution of magnetization for the complete time of the experiment. One minute after starting this continuous dc measurement, the field was set to zero with maximum available rate of 200 Oe s^{-1} (i.e. takes 50 seconds to go from -1 T to zero field). After 1 h, the temperature was increased to 2.5 K and the field was set again to -1 T. The field was then again set to zero field with 200 Oe s^{-1} and the evolution of magnetization was then tracked in zero field at 2.5 K. This procedure was repeated up to 5.5 K. **Figure S17** shows how the temperature *T*, the magnetic field *H* were changed over time and how the measured magnetization evolved accordingly (here only the measurement up to 5 K is shown). **Figure S18** left side presents the raw data of magnetization over time (for each temperature starting at the time when the field has reached zero). With the used 9 T PPMS from Quantum Design, it is known (see Application Note1070-207 from Quantum Design) that in the low field range (below 1 T) fields can only be set with an accuracy of about ±20 Oe due to magnetic flux line pinning. As a consequence, instead of a nominal zero field, a small positive field of up to 20 Oe might still be present as appeared by the small positive end magnetization for temperatures above 4 K. For better data handling, this effect has been compensated by shifting all raw data along $-y$-direction by the same value so that the final value of the 5.5 K curve matches zero magnetization (see **Figure S18** right side). These processed data sets are used for the plots in **Figure 7d** in the main text for further evaluation.

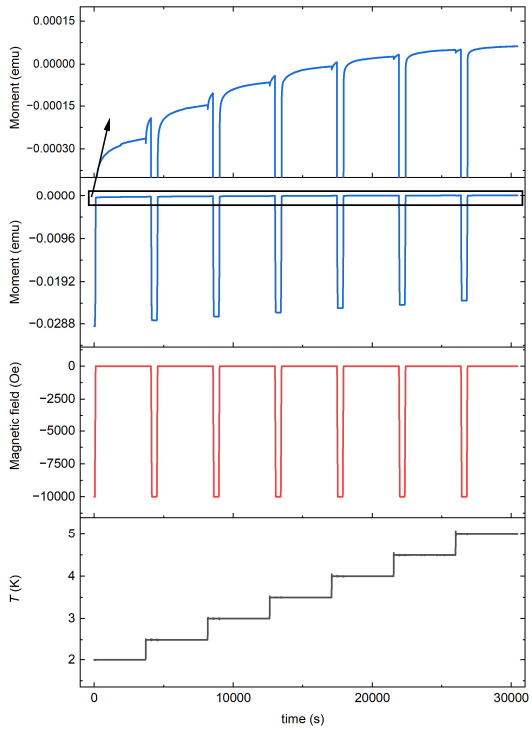

Figure S17. Time evolution of temperature *T*, magnetic field *H*, and measured magnetization *M* for complex **2**.

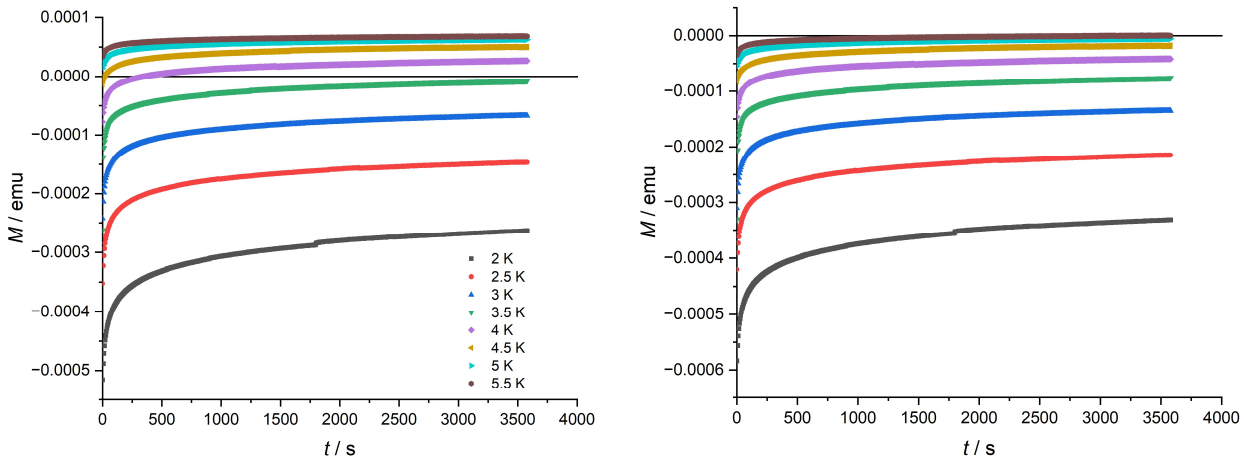

Figure S18. Left: Raw data of measured magnetization *M* for complex **2** over time at various temperatures. Right: Processed data where all curves have been shifted along −*y*-direction so that the final value of the 5.5 K curves matches zero magnetization.

15.Ground state optimization for complex 2

Table S6. Ground state total energy for different spin multiplicities (a.u.), expectation values for the $\langle S^2 \rangle$, as well as its deviation from the ideal value.

DFT	Spin	Expectation Value of $\langle S^2 \rangle$	Ideal Value of $\langle S^2 \rangle$	Deviation	Absolute Energy (a.u.)	Relative Energy (a.u.)	Relative Energy (cm^{-1})
B3LYP	S = 1/2	4.314715	0.750000	3.564715	-8379.38772606	0.10591594	23245.87
	S = 3/2	6.341763	3.750000	2.591763	-8379.38829141	0.10535059	23121.79
	S = 5/2	10.351976	8.750000	1.601976	-8379.42730811	0.06633389	14558.61
	S = 7/2	16.362146	15.750000	0.612146	-8379.46632191	0.02732010	5996.07
	S = 9/2	24.760604	24.750000	0.010604	-8379.49364200	0.00000000	0.00
PBE	S = 1/2	4.313665	0.750000	3.563665	-8377.04659938	0.05524246	12124.32
	S = 3/2	6.321046	3.750000	2.571046	-8377.01539342	0.08644842	18973.24
	S = 5/2	10.332048	8.750000	1.582048	-8377.04769696	0.05414488	11883.43
	S = 7/2	16.343123	15.750000	0.593123	-8377.07999286	0.02184898	4795.30
	S = 9/2	24.759138	24.750000	0.009138	-8377.10184184	0.00000000	0.00
TPSS0	S = 1/2	4.414255	0.750000	3.664255	-8380.67391544	0.12592115	27636.51
	S = 3/2	6.437626	3.750000	2.687626	-8380.67467006	0.12516653	27470.89
	S = 5/2	10.443671	8.750000	1.693671	-8380.71931591	0.08052068	17672.25
	S = 7/2	16.449678	15.750000	0.699678	-8380.76395639	0.03588020	7874.80
	S = 9/2	24.759906	24.750000	0.009906	-8380.79983659	0.00000000	0.00
wB97	S = 1/2	4.315024	0.750000	3.565024	-8380.78967631	0.10543829	23141.04
	S = 3/2	6.325446	3.750000	2.575446	-8380.78939185	0.10572275	23203.47
	S = 5/2	10.339251	8.750000	1.589251	-8380.82891153	0.06620307	14529.90
	S = 7/2	16.353034	15.750000	0.603034	-8380.86843143	0.02668317	5856.28
	S = 9/2	24.761045	24.750000	0.011045	-8380.89511460	0.00000000	0.00

Table S7. Loewdin charge and spin population analysis on main atoms, B3LYP, S = 9/2.

atom	Charge	Spin

Co	0.565714	2.769662
Co	0.269970	2.733919
Co	0.269970	2.733919
O	-0.398440	0.089422
O	-0.398440	0.089422
O	-0.405583	0.088118
O	-0.405583	0.088118
Cl	-0.419863	0.074581
Cl	-0.419863	0.074580
Cl	-0.424756	0.070782
Cl	-0.424756	0.070782
O	-0.066000	0.024411
O	-0.066000	0.024411
Si	0.567388	0.012097
Si	0.567388	0.012097
Si	0.576215	0.012014
Si	0.576216	0.012014
O	-0.306382	0.004099
O	-0.306382	0.004099

Table S8. Ground state total energy for different spin multiplicities (a.u.) for each Co site (using Co_1Zn_2 equivalents of Co_3 dianion), Co1 site, central.

DFT	Spin	Absolute Energy (a.u.)	Relative Energy (a.u.)	Relative Energy (cm^{-1})
B3LYP	$S = 1/2$	-9172.544757	0.02676550	5874.35
	$S = 3/2$	-9172.571523	0.00000000	0.00
PBE	$S = 1/2$	-9170.104545	0.01974838	4334.27
	$S = 3/2$	-9170.124294	0.00000000	0.00
TPSS0	$S = 1/2$	-9173.801943	0.03541389	7772.45
	$S = 3/2$	-9173.837357	0.00000000	0.00
wB97	$S = 1/2$	-9174.070628	0.02624608	5760.35
	$S = 3/2$	-9174.096874	0.00000000	0.00

Table S9. Ground state total energy for different spin multiplicities (a.u.) for each Co site (using Co_1Zn_2 equivalents of Co_3 dianion), Co2 site, terminal.

DFT	Spin	Absolute Energy (a.u.)	Relative Energy (a.u.)	Relative Energy (cm^{-1})
B3LYP	$S = 1/2$	-9172.525012	0.03889662	8536.82
	$S = 3/2$	-9172.563909	0.00000000	0.00
PBE	$S = 1/2$	-9170.088184	0.03229550	7088.05
	$S = 3/2$	-9170.120480	0.00000000	0.00
TPSS0	$S = 1/2$	-9173.783758	0.04449789	9766.16
	$S = 3/2$	-9173.828256	0.00000000	0.00
wB97	$S = 1/2$	-9174.048203	0.03942156	8652.04
	$S = 3/2$	-9174.087625	0.00000000	0.00

16.Multireference calculations for individual Co sites in Co_3 dianion

We used OpenMOLCAS, CASSCF, and CASPT2 methods to compute the low-lying energy structure for individual Co sites in the Co_3 dianion **2**.

Table S10. Low-lying energy structure on central Co1 site in different computational models, in cm^{-1}.

MB-CAS-7in5	VTZP-CAS-7in5	VTZP-CAS-7in10	VTZP-PT2-7in10
0.0	0.0	0.0	0.0
0.0	0.0	0.0	0.0
233.6	242.0	230.0	135.2
233.6	242.0	230.0	135.2
555.0	578.5	560.1	597.3
555.0	578.5	560.1	597.3
948.9	980.1	929.6	811.9
948.9	980.1	929.6	811.9
1143.5	1275.0	1278.1	1196.4
1143.5	1275.0	1278.1	1196.4
1317.3	1454.2	1435.2	1273.0
1317.3	1454.2	1435.2	1273.0
5293.1	5045.4	5381.9	5644.6
5293.1	5045.4	5381.9	5644.6
5374.2	5143.8	5466.5	5714.9
5374.2	5143.8	5466.5	5714.9
8251.9	7006.8	7446.1	8145.4
8251.9	7006.8	7446.1	8145.4
8292.4	7062.7	7490.1	8177.0
8292.4	7062.7	7490.1	8177.0
8597.2	7316.8	7766.7	8540.5
8597.2	7316.8	7766.7	8540.5
8727.8	7473.1	7899.2	8647.7
8727.8	7473.1	7899.2	8647.7

10696.4	13281.8	13704.9	9119.3
10696.4	13281.8	13704.9	9119.3
…	…	…	…

Table S11. Main values of the *g* tensor for the ground and first excited Kramers doublet within the formalism of pseudospin $S = 1/2$ for the central Co1 site.

MB-CAS-7in5	VTZP-CAS-7in5	VTZP-CAS-7in10	VTZP-PT2-7in10
$g_x = 1.7770$	$g_x = 1.7322$	$g_x = 1.7014$	$g_x = 1.7629$
$g_y = 1.9726$	$g_y = 1.9076$	$g_y = 1.8245$	$g_y = 2.5379$
$g_z = 8.3013$	$g_z = 8.4287$	$g_z = 8.4223$	$g_z = 7.3492$
$g_x = 3.9292$	$g_x = 3.8661$	$g_x = 3.8858$	$g_x = 2.1278$
$g_y = 3.4733$	$g_y = 3.6249$	$g_y = 3.6025$	$g_y = 2.2064$
$g_z = 1.7053$	$g_z = 1.6991$	$g_z = 1.7931$	$g_z = 5.3353$

Table S12. Main values of the *g* tensor for the ground Kramers doublet within the formalism of pseudospin $S = 3/2$ for the central Co1 site. Zero-field splitting parameters are also listed.

MB-CAS-7in5	VTZP-CAS-7in5	VTZP-CAS-7in10	VTZP-PT2-7in10
Main values of the *g* tensor for the ground $S = 3/2$			
$g_x = 1.9663$	$g_x = 1.9754$	$g_x = 1.9872$	$g_x = 2.0108$
$g_y = 2.0718$	$g_y = 2.0816$	$g_y = 2.0453$	$g_y = 2.3379$
$g_z = 3.1514$	$g_z = 3.1890$	$g_z = 3.1697$	$g_z = 2.7946$
$g_{iso} = 2.4556$	$g_{iso} = 2.4769$	$g_{iso} = 2.4617$	$g_{iso} = 2.4028$
Zero-Field Splitting parameters, D, E for the ground $S = 3/2$ term			
$D = -103.905$	$D = -108.629$	$D = -103.760$	$D = 60.439$
$E = -30.839$	$E = -30.779$	$E = -28.652$	$E = -17.543$

$$g_{iso} = \sqrt{\frac{g_x^2 + g_y^2 + g_z^2}{3}}$$

Table S13. Multi-configurational wavefunction description and their contribution towards *D* and *E*/*D* parameters for the central Co1 ion in complex **2**.

Energy (cm^{-1})	d_{z2}	d_{xz}	d_{yz}	d_{x2-y2}	d_{xy}	Weight (%)	Contribution towards D_{oh} (cm^{-1})	Contribution towards E_{oh} (cm^{-1})
0.0	1	2	1	2	1	64%	0.0	0.00
	2	2	1	1	1	34%		
290.6	1	2	1	1	2	90%	-129.98	-0.001
	2	1	2	1	1	6.4%		
852.2	2	1	1	1	2	93%	18.82	-18.84
	1	1	1	2	2	3.3%		
4573.7	2	1	1	2	1	99%	12.44	12.54
	2	1	1	1	2	0.46%		
6634.0	1	2	2	1	1	52.6%	6.81	-6.75
	1	1	1	2	2	23.7%		

For the central Co^{II} ion in an octahedral environment, the SA-CASSCF analysis reveals that the first excitation occurs within the same $|m_L|$ value, specifically from d_{x2-y2} to d_{xy}, with a small energy gap of 290.6 cm^{-1}. This transition significantly contributes to *D* with a value of -129.98 cm^{-1}. The second and third excitations involve transitions between different $|m_L|$ values, occurring at higher energy gaps of 852.2 cm^{-1} and 4573.7 cm^{-1}, contributing positively to *D* with values of 18.82 cm^{-1} and 12.44 cm^{-1}, respectively. These contributions explain the high absolute *D* value of approximately -100 cm^{-1} observed for the central Co^{II} ion in octahedral coordination.

Table S14. Low-lying energy structure on Co2 site in different computational models, in cm^{-1}.

MB-CAS-7in5	VTZP-CAS-7in5	VTZP-CAS-7in10	VTZP-PT2-7in10
0.0	0.0	0.0	0.0
0.0	0.0	0.0	0.0
55.5	60.2	56.6	43.8
55.5	60.2	56.6	43.8
1892.5	1753.9	1785.1	1912.1
1892.5	1753.9	1785.1	1912.1
2067.9	1965.3	1972.9	2041.7
2067.9	1965.3	1972.9	2041.7
3327.5	2913.8	3115.5	3842.4
3327.5	2913.8	3115.5	3842.4
3573.1	3190.1	3367.0	4015.6
3573.1	3190.1	3367.0	4015.6
4136.2	3754.5	3934.5	4629.8
4136.2	3754.5	3934.5	4629.8
4325.6	3964.7	4124.8	4681.2
4325.6	3964.7	4124.8	4681.2
5309.6	4569.4	4740.3	5381.3
5309.6	4569.4	4740.3	5381.3
5354.8	4637.8	4799.0	5415.3
5354.8	4637.8	4799.0	5415.3
6649.4	5779.9	5940.8	6621.1
6649.4	5779.9	5940.8	6621.1
6896.2	6122.6	6255.9	6845.1
6896.2	6122.6	6255.9	6845.1
7632.0	6598.2	6730.7	7362.0
7632.0	6598.2	6730.7	7362.0
7788.6	6832.6	6946.7	7551.5
7788.6	6832.6	6946.7	7551.5

Table S15. Main values of the *g* tensor for the ground and first excited Kramers doublets within the formalism of pseudospin $S = 1/2$ for the Co2 site.

MB-CAS-7in5	VTZP-CAS-7in5	VTZP-CAS-7in10	VTZP-PT2-7in10
$g_x = 0.4059$	$g_x = 0.5111$	$g_x = 0.4174$	$g_x = 1.7342$
$g_y = 0.4380$	$g_y = 0.5665$	$g_y = 0.4503$	$g_y = 2.6236$
$g_z = 7.7271$	$g_z = 7.9042$	$g_z = 7.8301$	$g_z = 6.4909$
$g_x = 4.8556$	$g_x = 5.0594$	$g_x = 4.9221$	$g_x = 1.6325$
$g_y = 4.0931$	$g_y = 4.0760$	$g_y = 4.1346$	$g_y = 1.9489$
$g_z = 2.6300$	$g_z = 2.7078$	$g_z = 2.6787$	$g_z = 6.0671$

Table S16. Main values of the *g* tensor for the ground Kramers doublet within the formalism of pseudospin $S = 3/2$ for the Co2 site. Zero-field splitting parameters are also listed.

MB-CAS-7in5	VTZP-CAS-7in5	VTZP-CAS-7in10	VTZP-PT2-7in10
Main values of the *g* tensor for the ground $S = 3/2$			
$g_x = 2.2296$	$g_x = 2.2800$	$g_x = 2.2588$	$g_x = 2.1683$
$g_y = 2.2759$	$g_y = 2.3374$	$g_y = 2.3054$	$g_y = 2.2884$
$g_z = 2.5932$	$g_z = 2.6613$	$g_z = 2.6295$	$g_z = 2.4520$
$g_{iso} = 2.3718$	$g_{iso} = 2.4321$	$g_{iso} = 2.4036$	$g_{iso} = 2.3059$
Zero-Field Splitting parameters, D, E for the ground $S = 3/2$ term			
$D = -27.592$	$D = -29.879$	$D = -28.161$	$D = 19.761$
$E = -1.718$	$E = -2.320$	$E = -1.778$	$E = -5.496$

$$g_{iso} = \sqrt{\frac{g_x^2 + g_y^2 + g_z^2}{3}}$$

Table S17. Multi-configurational wavefunction description and their contribution towards *D* and *E*/*D* parameter for the terminal Co2 ion in complex **2**.

Energy (cm^{-1})	d_{z2}	d_{xz}	d_{yz}	d_{x2-y2}	d_{xy}	Weight (%)	Contribution towards D_{Td}	Contribution towards E_{Td}

							(cm^{-1})	(cm^{-1})
0.0	2	1	1	1	2	97.3%	0.0	0.00
	2	1	1	2	1	1.7%		
1668.4	2	1	1	2	1	97.8%	-63.04	-0.01
	2	1	1	1	2	1.7%		
3016.1	1	2	1	1	2	75.6%	15.88	-13.55
	2	1	2	1	1	10.3%		
3524.2	1	2	1	2	1	55.6%	5.32	4.94
	2	2	1	1	1	33.5%		
4337.5	1	1	2	1	2	73.3%	10.44	7.178
	1	2	1	2	1	21.1%		

A similar analysis can be applied to the terminal Co^{II} ion in a tetrahedral environment. The negative D_{Td} arises due to spin-orbit coupling (SOC), primarily influenced by contributions from the dominant first excited state, which lies at 1668.4 cm^{-1} and is destabilized relative to the ground electronic state. This first excitation predominantly involves the electronic transition $d_{x2-y2} \rightarrow d_{xy}$ within the same $|m_L|$ level, with a D value of -63.04 cm^{-1}. Additionally, the second and third excitations occur between different $|m_L|$ values, with higher energy separations of 3016.1 cm^{-1} and 3524.2 cm^{-1}, respectively. These transitions contribute positively to D with values of 15.88 cm^{-1} and 5.32 cm^{-1}. Collectively, these effects account for the observed negative D value of approximately -29 cm^{-1} in the tetrahedral terminal Co^{II} ion.

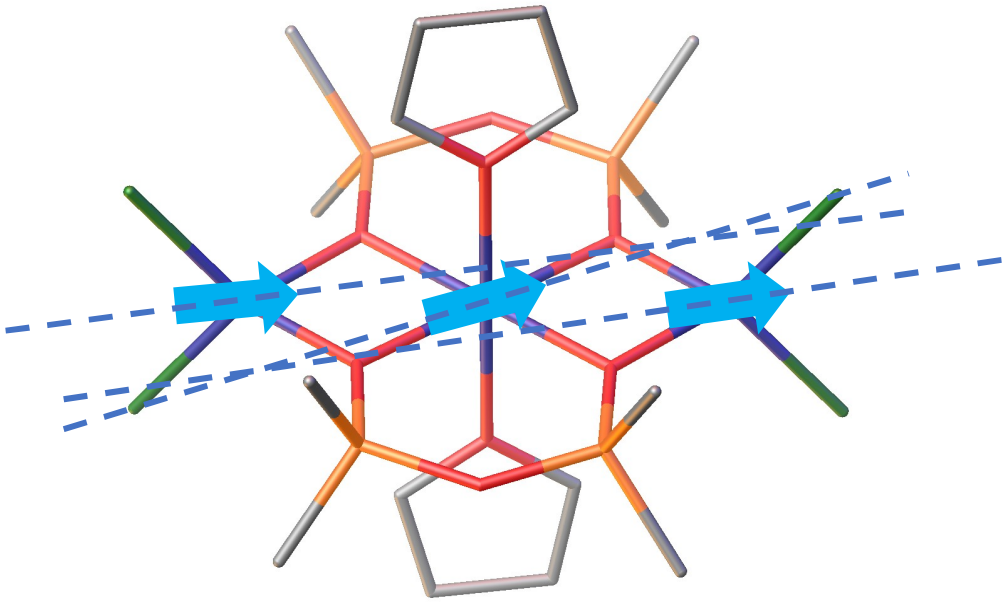

Figure S19. *Ab initio* calculated main anisotropy axes and ferromagnetic orientation (blue arrows) of the local magnetic moments in the ground energy state of **2**.

17. Broken-Symmetry evaluation of the magnetic exchange interactions

Table S18. Spin expectation values, deviations, and magnetic exchange coupling (J) for various theoretical levels in Co-Co interactions.

Interaction	Theory Level	S (High Spin)	$\langle S^2 \rangle$ (High Spin)	Ideal $\langle S^2 \rangle$ ($S = 3$)	Deviation (High Spin)	$\langle S^2 \rangle$ (BrokenSym)	Deviation (Broken Symmetry)	J (cm^{-1})
Co1-Co2	B3LYP	3	12.007	12	0.007	3.006	3.006	12.1
Co1-Co2	PBE	3	12.006	12	0.006	2.563	2.563	1322.77
Co1-Co2	TPSS0	3	12.006	12	0.006	3.006	3.006	9.27
Co1-Co2	wB97	3	12.007	12	0.007	3.007	3.007	10.23
Co1-Co2'	B3LYP	3	12.007	12	0.007	3.006	3.006	12.1
Co1-Co2'	PBE	3	12.006	12	0.006	2.563	2.563	1322.77
Co1-Co2'	TPSS0	3	12.006	12	0.006	3.006	3.006	9.27
Co1-Co2'	wB97	3	12.007	12	0.007	3.007	3.007	10.23

Co2-Co2'	B3LYP	3	12.008	12	0.008	3.008	3.008	-0.03
Co2-Co2'	PBE	3	12.007	12	0.007	2.956	2.956	1602.97
Co2-Co2'	TPSS0	3	12.007	12	0.007	3.007	3.007	-0.03
Co2-Co2'	wB97	3	12.008	12	0.008	3.008	3.008	-0.03

The PBE results cannot be trusted. In addition, the nearest-neighbor interaction is ferromagnetic, while the interaction between edges is much weaker and antiferromagnetic.

18.Lines model description of the magnetization (POLY-ANISO)

For the POLY-ANISO calculations, the exchange Hamiltonian is built using products of low-lying local spin-orbit states as basis functions. In this respect, eight (8) low-lying spin-orbit energy states as basis functions were used for Co1 (central), and six (6) low-lying spin-orbit energy states were used as basis functions for the terminal Co2. As such, the total size of the exchange Hamiltonian is 288. The total magnetic Hamiltonian is a sum of two terms: Lines exchange and dipole-dipole coupling. Diagonalization of the full Hamiltonian resulted in 288 coupled exchange states which were further used to describe the magnetic properties.

Table S19. Low-lying exchange energy spectra of **2**.

Exchange-only	Dipolar-only	Total (relative to ground state)
-39.84441501	-0.77246608	0.00000000
-39.84441501	-0.77246608	0.00000000
-9.29389357	0.03726451	31.32427443
-9.29389356	0.03726451	31.32427443
-5.17474783	0.04063378	35.37163032
-5.17474783	0.04063378	35.37163033
15.83762776	0.68738844	56.41818734
15.83762777	0.68738844	56.41818735
19.89965321	43.37709592	60.32251841

19.89965322	43.37709592	60.32251842
25.49560987	43.39418145	65.97197286
25.49560988	43.39418145	65.97197286
30.38675398	43.61250519	70.98776475
30.38675399	43.61250519	70.98776476
31.41755943	43.62610444	72.07212889
31.41755944	43.62610444	72.07212890
49.29517437	44.13233719	90.20713607
49.29517438	44.13233719	90.20713609
54.04916463	44.14717172	94.97350576
54.04916464	44.14717172	94.97350577
63.44515174	44.32355345	104.40146701
63.44515174	44.32355345	104.40146702
65.65955300	44.34163383	106.63934101
65.65955302	44.34163383	106.63934102
76.85159025	87.51633254	117.74037589
76.85159026	87.51633254	117.74037590
85.16005493	87.72639351	125.94188428
85.16005494	87.72639351	125.94188429
92.33342429	87.74795480	133.12497750
92.33342430	87.74795480	133.12497751
101.36881096	87.97097692	142.17226041
101.36881097	87.97097692	142.17226042
123.12982039	135.00443747	163.79483592
123.12982039	135.00443747	163.79483592
133.48993495	135.32430079	174.16806333
133.48993497	135.32430079	174.16806334
137.64985393	135.33705493	178.32071142
137.64985394	135.33705493	178.32071143
147.85822308	135.51645813	188.71266936
147.85822308	135.51645813	188.71266937

157.75426835	178.92600227	198.51651154
157.75426836	178.92600227	198.51651155
160.49755693	178.94876432	201.25554078
160.49755694	178.94876432	201.25554079
169.05553926	179.05143382	209.74690067
169.05553928	179.05143382	209.74690070
172.28142149	179.05923370	212.97086137
172.28142152	179.05923370	212.97086140
190.75427926	179.26755980	231.44825383
190.75427927	179.26755980	231.44825384
…	…	…
Main g_Z in the low-lying two exchange doublets		
Co1	g_X	0.24552
	g_Y	0.67162
	g_Z	21.37732
Co2	g_X	0.37223
	g_Y	3.63599
	g_Z	9.16509

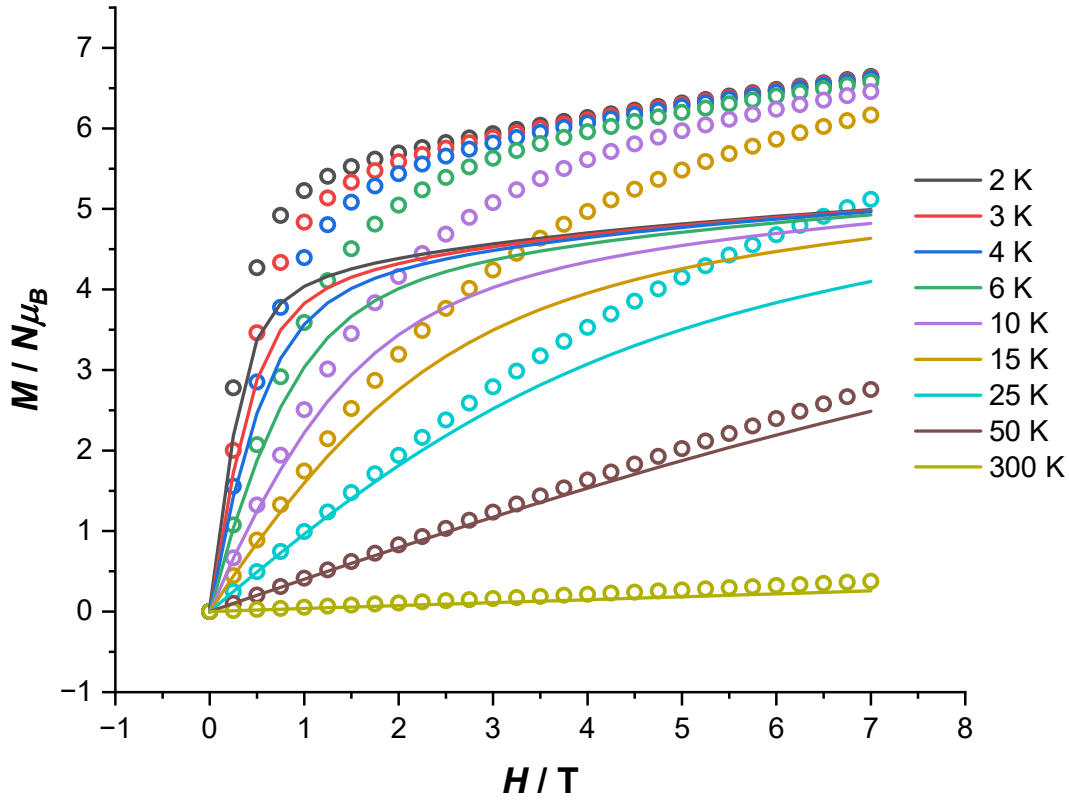

Figure S20. Magnetization (*M*) vs *H* plots for complex **2** at different temperatures. The solid lines represent the experimental data, and the circles represent the calculated results using the Lines model as described in the *ab initio* calculations section. The possible reasons for the discrepancy are given in the main text.

19.Additional ac susceptibility data

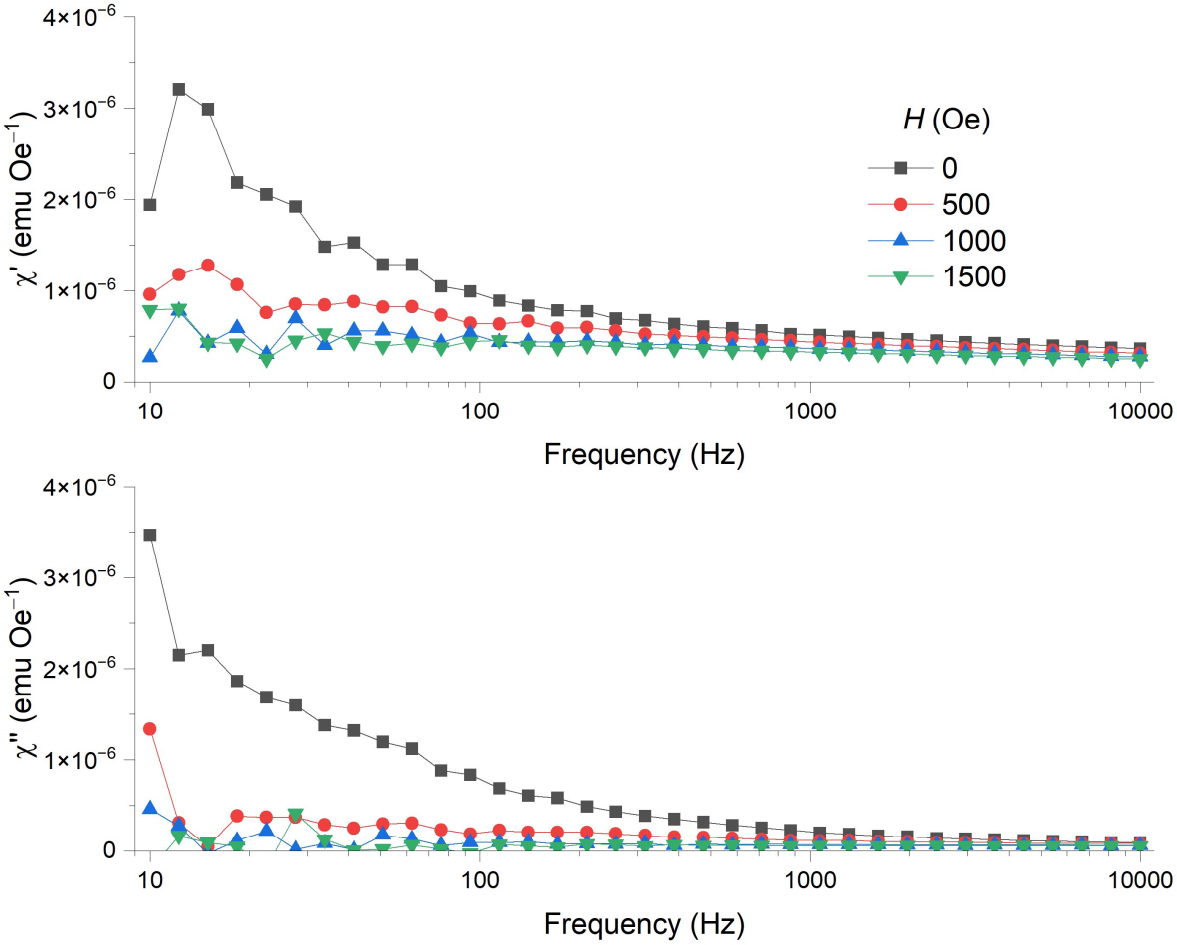

Figure S21. The ac susceptibility in-phase, χ' (above) and out-phase, χ'' (below) data for complex **2** measured from 10 Hz to 10 kHz at 35 frequencies with log-distribution at 0, 500, 1000, and 1500 Oe dc field at 2 K temperature.

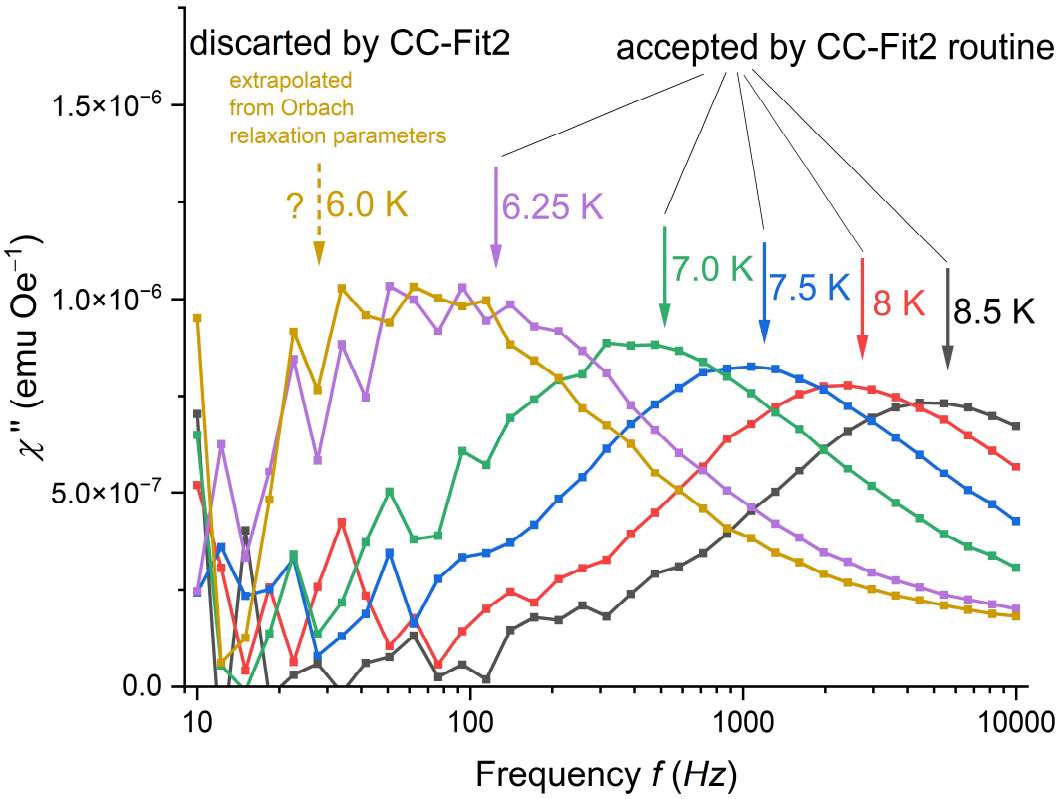

Figure S22. AC susceptibility χ'' curves for complex **2** for a selection of temperatures. At 8.5 K, the χ'' signal exhibits a clear maximum at the high end of available ac excitation frequency (10 kHz). In the main text, the evolution of this maximum with temperature is described for the temperatures 8.5, 8.25, 8.0, 7.75, 7.5, 7.25, 7.0, 6.75, 6.5, and 6.25 K (in the Figure only a selection of these temperatures is shown for clarity). However, for 6.0 K, the program CC-Fit2 discarded a fit by a generalized Debye function, because the maximum in the χ'' signal is not well defined any more. From the Orbach fit (that has been obtained by a fit to the relaxation times from 8.5 K to 6.25 K) the position of the expected χ'' signal for 6.0 K was calculated (see dashed arrow). It is obvious that for 6.0 K, the measured χ'' signal does not clearly show a maximum that is centered at this frequency. Since the noise in the χ'' signal strongly increases for lower frequencies, the relaxation times could only be determined down to 6.25 K. The low available sample mass of only 3.3 mg here also contributes to the noisy signal at low frequencies.

20.References

(1) Milios, C. J.; Prescimone, A.; Sanchez-Benitez, J.; Parsons, S.; Murrie, M.; Brechin, E. K. High-spin M^{2+} carboxylate triangles from the microwave. *Inorg. Chem.* **2006**, *45*, 7053–7055.

(2) Zabala-Lekuona, A.; Landart-Gereka, A.; Quesada-Moreno, M. M.; Mota, A. J.; Díaz-Ortega, I. F.; Nojiri, H.; Krzystek, J.; Seco, J. M.; Colacio, E. Zero-Field SMM Behavior Triggered by Magnetic Exchange Interactions and a Collinear Arrangement of Local Anisotropy Axes in a Linear Co_3^{II} Complex. *Inorg. Chem.* **2023**, *62*, 20030–20041.

(3) Zhang, Y.-Z.; Brown, A. J.; Meng, Y.-S.; Sun, H.-L.; Gao, S. Linear Trinuclear Cobalt(II) Single Molecule Magnet. *Dalton Trans.* **2015**, *44*, 2865–2870.

(4) Yang, Y.-T.; Zhao, F.-H.; Che, Y.-X.; Zheng, J.-M. A Unique Mixed-Bridged Trinuclear Co(II) Complex and Its Extended System: Structural and Magnetic Studies. *Inorg. Chem. Commun.* **2011**, *14*, 1802–1806.

(5) Malaestean, I. L.; Speldrich, M.; Baca, S. G.; Ellern, A.; Schilder, H.; Kögerler, P. Diphenic Acid-Based Cobalt(II) Complexes: Trinuclear and Double-Helical Structures. *Eur. J. Inorg. Chem.* **2009**, *2009*, 1011–1018.

(6) Monakhov, K. Yu.; van Leusen, J.; Kögerler, P.; Zins, E.; Alikhani, M. E.; Tromp, M.; Danopoulos, A. A.; Braunstein, P. Linear, Trinuclear Cobalt Complexes with *o* -Phenylene-bis-Silylamido Ligands. *Chem. – Eur. J.* **2017**, *23*, 6504–6508.

(7) Tomkowicz, Z.; Ostrovsky, S.; Müller-Bunz, H.; Eltmimi, A. J. H.; Rams, M.; Brown, D. A.; Haase, W. Extended Triple-Bridged Ni(II)- and Co(II)-Hydroxamate Trinuclear Complexes: Synthesis, Crystal Structures, and Magnetic Properties. *Inorg. Chem.* **2008**, *47*, 6956–6963.

(8) Suenaga, Y.; Nakaguchi, Y.; Fujishima, Y.; Konaka, H.; Okuda, K. Synthesis and Characterization of a Tri-Nuclear Co(II) Complex with a Bis(Catecholate) Ligand. *Inorg. Chem. Commun.* **2011**, *14*, 440–443.

(9) Yi, T.; Ho-Chol, C.; Gao, S.; Kitagawa, S. Tuning of the Spin States in Trinuclear Cobalt Compounds of Pyridazine by the Second Simple Bridging Ligand. *Eur. J. Inorg. Chem.* **2006**, *2006*, 1381–1387.

(10) Plaul, D.; Böhme, M.; Ostrovsky, S.; Tomkowicz, Z.; Görls, H.; Haase, W.; Plass, W. Modeling Spin Interactions in a Triangular Cobalt(II) Complex with Triaminoguanidine Ligand Framework: Synthesis, Structure, and Magnetic Properties. *Inorg. Chem.* **2018**, *57*, 106–119.

(11) Pang, Y.; Cui, S.; Li, B.; Zhang, J.; Wang, Y.; Zhang, H. Metal-Dependent Assembly of a Helical-[Co_3 L_3] Cluster versus a Meso-[Cu_2 L_2] Cluster with O,N,N′,O′-Schiff Base Ligand: Structures and Magnetic Properties. *Inorg. Chem.* **2008**, *47*, 10317–10324.

(12) Oldengott, J.; Stammler, A.; Bögge, H.; Glaser, T. Enhancing the Ferromagnetic Coupling in Extended Phloroglucinol Complexes by Increasing the Metal SOMO–Ligand Overlap: Synthesis and Characterization of a Trinuclear Co^{II}_3 Triplesalophen Complex. *Dalton Trans.* **2015**, *44*, 9732–9735.

(13) Mocanu, M. I.; Patrascu, A. A.; Hillebrand, M.; Shova, S.; Lloret, F.; Julve, M.; Andruh, M. Trinuclear Nickel(II) and Cobalt(II) Complexes Constructed from Mannich–Schiff-Base Ligands: Synthesis, Crystal Structures, and Magnetic Properties. *Eur. J. Inorg. Chem.* **2019**, *2019*, 4773–4783.